POLITECNICO DI MILANO

School of Industrial and Information Engineering

Master of Science Degree in
Space Engineering

ROBUSTNESS ANALYSIS OF BALLISTIC CAPTURE ORBITS IN THE ELLIPTIC RESTRICTED THREE-BODY PROBLEM

Supervisor:
Prof. Francesco TOPPUTO

M.Sc. Thesis of:
Marco D. CAIAZZO
Matr. 816237

Academic Year 2015 – 2016

Alla mia mamma, al mio papà
ed alla mia nonna, che hanno
reso tutto questo possibile.

TABLE OF CONTENTS

LIST OF FIGURES

LIST OF TABLES

ABSTRACT

The techniques exploited in finding preliminary trajectories for interplanetary space flights have been, during these last years, widely studied and improved. The motivations of these developments are related to the necessity of studying those complex phenomena occurring when more gravitational interactions are considered together. One of them is represented by the so called *ballistic capture*, which can be explained when at least two *primaries* considered. In this thesis, the robustness of ballistic capture orbits is assessed. The primary system considered the Sun-Mars one. In particular, a statistical approach is exploited to generate families of initial conditions in order to reproduce the common uncertainties of position and velocities related to deep space navigation. This leads to more or less substantial shifting with respect to the nominal condition. As consequence there will be some non-acceptable conditions for a ballistic capture. Therefore, results are presented in terms of robust initial conditions and non-robust one, that is leading to crash over the surface of Mars or escape from it Sphere of Influence.

SOMMARIO

Le tecniche utilizzate nella ricerca di traiettorie preliminari per voli spaziali interplanetari sono state, nel corso di questi ultimi anni, ampiamente studiate e migliorate. Le ragioni di tali miglioramenti sono legate soprattutto alla necessitàdi ptoer studiare quei particolari fenomeni che si verificano quando più interazioni gravitazionali si trovano in essere. Uno di questi è rappresetato dalla cosiddetta *cattura balistica*, che trova spiegazione nella considerazione di almeno due *primari*. In questa tesi verrà verificata la robustezza delle catture balistiche. Il sistema di primari considerato è Sole-Marte. In particlare, verranno generate famiglie di condizioni iniziali con un approccio statistico, così da riprodurre i comuni livelli di incertezza associati alla navigazione spaziale. Questo comporta variazioni più o meno consistenti rispetto alla condizione nominale e, di conseguenza, non tutte le condizioni ottenute saranno accettabili al fine di effettuare una cattura balistica. Pertanto i risultati saranno presentati in termini di condizioni iniziali robuste e non rouste, ovvero provocanti uno schianto sulla superficie di Marte od una fuga dalla sua Sfera di Influenza.

RINGRAZIAMENTI

Desidero ringraziare prima di tutto il Prof. Topputo per avermi concesso la possibilità di portare avanti questo lavoro di tesi e, nel contempo, affacciarmi sul mondo del lavoro. Un sentito ringraziamento per la sua incredibile disponibilità e per tutti gli inestimabili consigli durante lo sviluppo di questa tesi. Un caloroso grazie anche al prof. Di Lizia per la grande disponibilità mostrata nel fugare tutti i miei dubbi e per i preziosi suggerimenti per lo svolgimento del lavoro.

Di compagni di viaggio ce ne sono stati molti in questi anni. Ciascuno di essi ha contribuito a rendere questa parte della mia vita davvero unica. Ringrazio tutti i colleghi del Politecnico che ho incontrato in questo percorso di studi, e di vita. Chris, Mirko, Seba, Teo: abbiamo iniziato insieme. Con voi ho mosso i primi passi nel mondo dell'ingegneria. Voi avete reso questi anni davvero preziosi ed indimenticabili. Siete delle persone stupende. Leo, Capa, Fede, Roby, Aleb: è stato meraviglioso giungere alla fine di questo percorso al vostro fianco. Vi ringrazio per le innumerevoli serate all'insegna del divertimento in cui ne abbiamo combinate di ogni e grazie anche per aver reso le PK, con la vostra compagnia, un posto più bello. Devo ringraziare ancora due persone, le più importanti, a cui devo più di tutti.
Alessandro: senza di te non sarei mai arrivato a questo giorno. Ti ringrazio di cuore per essermi stato sempre vicino e per avermi sempre incoraggiato e per non avermi fatto mollare mai. Per me sei stato come un fratello, e lo sarai sempre.
Mavy: abbiamo condiviso soltanto due anni insieme, ma è come se ci conoscessimo da una vita. Sei una delle persone più belle e preziose che abbia mai incontrato. Un grazie di cuore per esserci stata sempre per me e per aver reso splendido questo tempo insieme. Sei una persona speciale e meriti tutto il meglio che la vita abbia da offrire.

Un grazie di cuore a tutti gli amici che hanno vissuto al mio fianco in questi anni.
Gio: da più di vent'anni condividiamo insieme tutte le sfide che la vita ha da offrirci. Sei un punto fisso nella mia vita e così sarà sempre.
Ali, Fra, Andre, Kos, Tino e Bobby: siete i migliori amici che si possano avere e sono felicissimo di aver condiviso, con chi più e con chi meno, questi bellissimi anni.
Un grazie di cuore va soprattutto ad Eleonora, Camilla e Rebecca: la vita ci ha fatto incontrare per caso ed è stata una delle cose più belle che potessero capitarmi. Vi ringrazio per avermi regalato quei momenti indimenticabili che abbiamo vissuto insieme e che non dimenticherò mai.

Più di tutto, oltre ogni cosa, il grazie più sentito e più grande va ai miei genitori. Grazie per avermi sempre sostenuto, incoraggiato ed aiutato a rialzarmi nei momenti più bui. Grazie per aver celebrato con me i successi fin'ora conseguiti e per avermi sempre incoraggiato a perseguire i miei sogni. Grazie per reso possibile, e finalmente reale, questo momento. Mamma, papà: senza di voi non ce l'avrei mai fatta. Questo giorno lo dedico a voi.

INTRODUCTION

The design of space missions is carried out, in general, through a series of iterations. Starting, in fact, from simplified models of the considered dynamic system, the process of defining the mission proceeds through different levels of analysis, each one leading to a more and more detailed characterization of all tge systems involved. During the ohase of *trade-off*, all the subsystems are relatd each other, therefore the development of on of them affects the entire mission design.

Altough it does not represent any physical components of the system, the mission analsis plays a role of utmost importance during the design phase, as different trajectories and orbits correspond to different spin-off for the other subsystems. As a consquence, a good level of precision in the characterization of the orbit, already in the preliminary phase, positevly influences the design procedure. For this reason, refined techniques are required, either deveipong the agorithms of computation, or using more detailed and complex models. A typical example is represented by interplanetary missions, where the trajectories are usually defined through the *patched conics* approach: by exploiting this technique, the complete trajectory made up by patching solutions of many two-body problem, each one considered when the spacecraft enters the Sphere of Influence of the relative planet. The advantage of this method is represented by the existence of an analytical solution of the problem but, at the same time, it implies a discontinuous motion across those imaginay boundaries produced by the Keplerian decomposition of the solar System. Together with this limitation, in the last decades, the attention fo the space agencies has been more and more oriented on searching those solutions where the consumption of mass of propellant is as low as possible. These type of solutions allow, for instance, to embark much propellant mass or, in general, to reduce the costs of the entire mission.

In this sense, the classic patched conics model is not really suitable in finding those trajectories satisfying the new mission requirements, because of their dynamics, too much simplified. Therefore, the necessity of studying different and more precise models becomes a priority, giving the possibility of understanding those complex phaeonoena not provided in the two-body simplification. The first steps towards this direction were done in the early 90s by E. Belbruno, who, in collaboration with J. MIller, found a new ype of trajectories studying a model where the interactions between the gravitational attraction of the Earth, the Sun and the Moon were taken in consideration *Belbruno* e *Miller* [3]. This results, which brought to definition of the so called *weak stability boundaries*, inspired detailed studies on the laws governing such motions. On of those, developed by W. Kon, M. LO, J. Marsden and S. Ross explains those trajectories separating the model analyzed by Belbruno and miller into two different restricted three body problems *Koon* et al. [11].

The restricted three-body probem represents in fact the model immediately successive, in complexity, to the two-body problem. When two primaries are considered

together, the interations of their gravitational fields and their efects on a third body, whose mass is negligible with respect to the first two, can be investigated. This model, which still represents an approximation of the dynamics occurring inside the Solar System, has as drawback the absence of any analytical solution but, starting from its equations of motion, some useful considertions can be still stated. An example are the Hill's regions, which define the limits in the motion of the third particle; furthemore, the presence of five equilibrium points (called *Lagrangian points*) opens new perspectives from the point of view of possible missions around them. It is demonstrated that, nearby such points, connections between different regions of motions are possible, if the energetic level is appropriate (*Belbruno* [1], *Koon* et al. [10]).

Using the restricted three-body problem, a description of the *weak stability boundaries*, with the related dynamics, can be performed. After its definition, the tchnique illustrated by Beltruno *et al.* has been in fact often considered when *ballistic capture trajectory* are searched. However the canonical circular restricted three-body problem represents a model in thich the real dynamics of the planets is stil too much simplified. The elliptic problem is therefore to prefer, since it leads to much more accurate results.

Its detailed description is reported in the first chapter, where the equations of motion are obtained and discussed: the main differences etween this model and the circular one are evident. The elliptic problem is, in fact, governed by a *non-autonomous* system of equations, where the independent variable (the true anomaly f) appears explicitly inside the equations. A constant of motion still exists, like in the circular problem, however the so-called *Jacobi constant*, in the elliptic one, cannot be used to define the Hill's region. In fact, when the elliptic problem is considered, such regions of motion exhibit a *pulsating behavior*. Moreover they can be estimated during the first instants of motion only, when some approximations are valid.

In the second chapter, the definitions of ballistic capture and escape, stable set and weak stability boundary are recalled and extended to the elliptic problem: in this case in fact, it is shown that for different initial values of the independent variable, different stable conditions can be found. Furthemore, the presence of *negative* stable sets is discussed making possible the definition of ballistic capture and and escape, when backward integration is performed. Like already demonstrated *Szebehely* [15], it will be showed how it is convenient to solve not directly the classic equations of motions, but those in polar coordinates. Furthemore, also a regularization of the system of equations appears necessary, in order to calculate quickly and with high precision, those trajectories passing near the singuarities of the equations.

Once this model has been discussed, in the third chapter the robustness analysis of the method is analyzed. After a brief discussion of the capture set, the statistical procedure producing a family of perturbed initial conditions. Consequently, such conditions are propagated and the behaviour of the resulting orbits in terms of effective capture, crashes and escapes is treated. The dispersion map of the State vector at fixed stages is also presented. Eventually, the last part of the chapter is devoted to the conclusions and the future development and improvement to this method will be discussed, such as the re-formulation of the problem by means

of *Differential algebra*, which is treated in *Wittig* et al. [18] and *Di Lizia*, *Armellin* e *Lavagna* [5].

1 ELLIPTIC RESTRICTED THREE-BODY PROBLEM

The elliptic restricted three-body problem stems from the circular formulation, which is deeply analyzed in literature. In particular, in this thesis the most outstanding reference is represented by *Szebehely* [15], according to whom:

> *"Two bodies revolve around their center of mass in circular orbits under the influence of their mutual gravitational attraction and a third body (attracted by the previous two but not influencing their motion) moves in the plane defined by the two revolving bodies. The restricted problem of three bodies is to describe the motion of this third body."*

Basing on this statement, the concept of *restricted* problem is clarified: the third body, which is nothing but the spacecraft, does not alter the dynamics of the first two ones, which are commonly labeled as *primaries*. This fact is fully justified in thinking that the gravitational force exerted by the spacecraft on the primaries is extremely small; as a consequence, its contribution to the dynamics of the overall system can be neglected. The most significant modification to Szebehely's model lies in considering the primaries paths as *elliptic*. The immediate consequence of this assumption is that their relative distance keeps no longer constant, but results in an oscillating, or *pulsating*, behavior. Of course a much more complicated analytical formulation is required, in particular the dependence on time needs a radical revision, but results are much improved since they are closer to the actual situation of celestial mechanics.

1.1 EQUATIONS OF MOTION

As already mentioned, the main difference between the classic restricted problem and the elliptic one consist in the presence of the orbit eccentricity when considering the motion of the primaries. In order to better understand how the orbital non-circularity enters the problem, the motion of the primaries needs to be investigated. While for the classic problem the revolution is circular around the system center of mass, in the case under analysis the motion around such point is elliptic and already known through the equations of the two-body problem. In the Solar System, all big planets revolve around the Sun and the associated mass ratio is such that this approximation can always be considered valid.

1.1.1 The Sidereal Reference Frame

In order to write the equations of motion it is necessary to specify a reference frame. A first choice is to define a coordinate system fixed to the center of gravity of the system made of the two primaries and preserving its orientation with respect to a fixed reference. Such reference is labeled as *sidereal* and it represented in Figure 1.1.

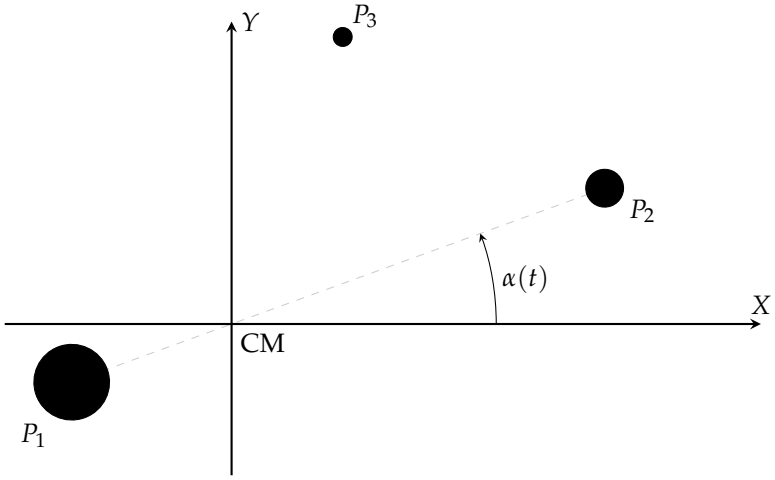

Figura 1.1: Sidereal baricentric reference frame.

The angle α between the line joining the primaries and the X-axis results from the summation of the true anomaly, which will be denoted with $f(t)$ and the pericenter anomaly of the second primary P_2 with respect to the first one P_1. Within the sidereal reference frame, the spacecraft position (P_3) is identified by the vector $\boldsymbol{R} = \begin{bmatrix} X & Y \end{bmatrix}$, while each primary is located at $\boldsymbol{R}_i = \begin{bmatrix} X_i & Y_i \end{bmatrix}$. Accordingly, the distance between the spacecraft and each primary is:

$$R_i^2 = (X - X_i)^2 + (Y - Y_i)^2$$

Once defined this quantity, the equation of motion of the spacecraft under the gravitational effect of P_1 and P_2 are:

$$\frac{d^2X}{dt^2} = -m_1 G \frac{X - X_1}{R_1^3} - m_2 G \frac{X - X_2}{R_2^3} \tag{1.1}$$

$$\frac{d^2Y}{dt^2} = -m_1 G \frac{Y - Y_1}{R_1^3} - m_2 G \frac{Y - Y_2}{R_2^3} \tag{1.2}$$

where G is the universal gravitational constant and m_1 and m_2 are, respectively, the masses of the first and the second primary. In eqs. (1.1) and (1.2) the dependence on time, which is the independent variable, appears through R_1 and R_2, which are time dependent due to the fact that an elliptic problem is being analyzed. A relation can

be pointed out between the true anomaly of the second primary and the time, that is the *Kepler equation* for time. Recalling the relation existing between $f(t)$ and the eccentric anomaly E:

$$\tan\left(\frac{f}{2}\right) = \sqrt{\frac{1+e}{1-e}}\tan\left(\frac{E}{2}\right) \tag{1.3}$$

where e is the eccentricity of the elliptic orbit of P_2 around P_1, the connection between f and t results from:

$$\sqrt{\frac{G\left(m_1+m_2\right)}{a^3}}\left(t-t_0\right) = E - e\sin\left(E\right) - \left(E_0 - e\sin\left(E_0\right)\right) \tag{1.4}$$

where the numerator of the term under square root is the mass parameter for the two-body problem and a is the semi-major axis of the considered elliptic orbit. By inverting eq. (1.4), the eccentric anomaly can be retrieved. Using this result inside equation 1.3 allows to compute the true anomaly. So the dependence on time of eqs. 1.1 and 1.2 has been explained.

1.1.2 The Synodic Reference Frame

From eqs. (1.1) and (1.2) it is evident that, within the sidereal reference frame, the equations of motion can be immediately obtained directly from gravitational contributions acting between the involved primaries. Despite this apparent simplicity, it must be taken into account that the primaries are not still and the distance existing between them does not keeps constant in time, thus increasing the difficulties in understanding the interactions occurring either between them and the spacecraft once the equations are solved. Due to these considerations, it should be used a reference frame such that primaries are fixed in space.

The reference that is being discussed features the x-axis coincident with the line joining the primaries and the y-axis directed perpendicularly in counterclockwise direction. The center of the frame is, once again, the center of mass of the system. Such system is called *synodic* and it is represented in Figure 1.2. Notice that the axes belonging to the sidereal one have not been removed for sake of clarity and in order to point out the difference between the two frames.

Practically speaking, a rotation is required to switch from a reference frame to the other one. For example, to switch from synodic to sidereal the operation to be performed is:

$$\begin{bmatrix} X \\ \\ Y \end{bmatrix} = \begin{bmatrix} \cos\left(\alpha(t)\right) & -\sin\left(\alpha(t)\right) \\ \\ \sin\left(\alpha(t)\right) & \cos\left(\alpha(t)\right) \end{bmatrix} \begin{bmatrix} x \\ \\ y \end{bmatrix} \tag{1.5}$$

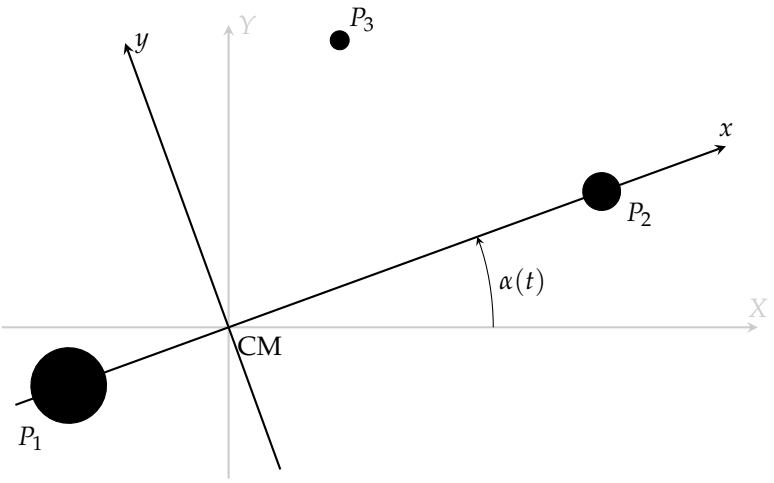

Figura 1.2: Synodic baricentric reference frame.

Thanks to the choice of this new reference frame it results that the primaries will always lie on the x-axis, which implies that $y_i = 0$ always. Accordingly, it is possible to define, as for the sidereal frame, the distance of the spacecraft from its attractors. Since the position vector of P_3 is $\boldsymbol{r} = \begin{bmatrix} x & y \end{bmatrix}$, it follows that:

$$r_i^2 = (x - x_i)^2 + y^2$$

Nevertheless, their distance is still varying in time due to the fact that they move along elliptic paths. Such varying distance can be retrieved from the two-body problem, according to which:

$$r(f) = \frac{a\left(1 - e^2\right)}{1 + e\cos\left(f\right)} \tag{1.6}$$

where a and e are, respectively, the semi-major axis and the eccentricity of the orbit of the second primary P_2 around the first one P_1 and e. The non-constant value of r can be deduced immediately from its dependence on f which, in turn, is function of time.

To overcome this issue and have fixed and constant distance, a further transformation involving complex numbers is required. The following quantities are defined:

$$Z = ze^{j\alpha} \qquad \text{with} \qquad \begin{array}{rcl} Z & = & X + jY \\ z & = & x + jy \end{array}$$

through which equations of motion become:

$$\frac{d^2Z}{d^2t} = -G\frac{m_1}{r_1^3}(Z - Z_1) - G\frac{m_2}{r_2^3}(Z - Z_2) \tag{1.7}$$

By analyzing separately the left and the right-hand terms some considerations can be performed. By applying the definition of Z on the second order derivative, it can be rewritten as:

$$\frac{d^2Z}{d^2t} = \frac{d^2z}{dt^2}e^{j\alpha} + 2j\frac{dz}{dt}e^{j\alpha} + jz\frac{d^2f}{d^2t}e^{j\alpha} - z\left(\frac{df}{dt}\right)^2 e^{j\alpha} \tag{1.8}$$

Due to the fact that a non-inertial reference frame is being treated, there are some terms expressing the acceleration. They are, in order of appearance, the radial, Coriolis', tangential and centrifugal effects.

The second step consist in making the problem non-dimensional. Accordingly, the non-dimensional complex coordinate ζ is obtained as:

$$\zeta = \frac{z}{r} \qquad \longrightarrow \qquad z = r\zeta$$

The first and second order derivatives of z become:

$$\begin{aligned}\frac{dz}{dt} &= \zeta\frac{dr}{dt} + r\frac{d\zeta}{dt}\\ \frac{d^2z}{dt^2} &= \zeta\frac{d^2r}{dt^2} + 2\frac{dr}{dt}\frac{d\zeta}{dt} + r\frac{d^2\zeta}{dt^2}\end{aligned}$$

In turn, the time derivatives of ζ can be rewritten in terms of true anomaly. Since $\zeta = \zeta(f(t))$ it follows that:

$$\begin{aligned}\frac{d\zeta}{dt} &= \frac{d\zeta}{df}\frac{df}{dt}\\ \frac{d^2\zeta}{dt^2} &= \frac{d^2\zeta}{df^2}\left(\frac{df}{dt}\right)^2 + \frac{d\zeta}{df}\frac{d^2\zeta}{dt^2}\end{aligned}$$

Consequently the ultimate form of the first and second elements of the right-hand term of equation 1.8 become:

$$\frac{d^2z}{dt^2} = r\left[\frac{d\zeta}{df}\frac{d^2f}{dt^2} + \frac{d^2\zeta}{df^2}\left(\frac{df}{dt}\right)^2\right] + 2\frac{dr}{dt}\frac{d\zeta}{df}\frac{df}{dt} + \zeta\frac{d^2r}{dt^2} \tag{1.9}$$

$$2j\frac{dz}{dt} = 2j\left[\frac{dr}{dt}\frac{df}{dt} + r\frac{d\zeta}{df}\left(\frac{df}{dt}\right)^2\right] \tag{1.10}$$

Before merging the results, the gravitational contributions must be analyzed. By exploiting the definition of Z and by taking the non-dimensional form, the right-hand side of equation 1.7 becomes:

$$\begin{aligned} -G\frac{m_1}{r_1^3}(Z-Z_1) - G\frac{m_2}{r_2^3}(Z-Z_2) &= -G\frac{m_1}{r_1^3}(z-z_1)\,e^{j\alpha} - G\frac{m_2}{r_2^3}(z-z_2)\,e^{j\alpha} \\ &= -G\frac{m_1}{r_1^3 r^2}(\zeta-\zeta_1)\,e^{j\alpha} - G\frac{m_2}{r_2^3 r^2}(\zeta-\zeta_2)\,e^{j\alpha} \end{aligned} \tag{1.11}$$

Now it is possible to write the non-dimensional, complex-form equations of motion putting together equations 1.8, 1.9, 1.10 and 1.11:

$$\begin{aligned} &r\left(\frac{df}{dt}\right)^2\left[\frac{d^2\zeta}{df^2}+2j\frac{d\zeta}{df}\right]+\zeta\left[\frac{d^2r}{dt^2}-r\left(\frac{df}{dt}\right)^2\right]+ \\ &\quad+\left(\frac{d\zeta}{df}+j\zeta\right)\left(r\frac{d^2f}{dt^2}+2\frac{dr}{dt}\frac{df}{dt}\right) = -G\frac{m_1}{r^2r_1^3}(\zeta-\zeta_1) - G\frac{m_2}{r^2r_2^3}(\zeta-\zeta_2) \end{aligned} \tag{1.12}$$

The next step consists in "replacing" the dependence on time with the one on true anomaly. To do so, from the definition of the angular momentum:

$$\|\boldsymbol{h}\|^2 = \left(r^2\frac{df}{dt}\right)^2 \tag{1.13}$$

by taking its time derivative and setting it to zero it is possible to get rid of the third element of the left-hand term of equation 1.12. This assumption is justified due to the fact that no perturbation has been considered, therefore both the direction and the magnitude of the angular momentum vector keep constant.

$$2\left(r^2\frac{df}{dt}\right)\left(2r\frac{dr}{dt}\frac{df}{dt}+r\frac{d^2f}{dt^2}\right) = 0 \tag{1.14}$$

The following step consist in write an alternate form of the second term of the left-hand term of eq. (1.12). In fact, it represent the radial component of the acceleration vector. So:

$$\begin{aligned} \frac{d^2r}{dt^2}-r\left(\frac{df}{dt}\right)^2 &= -G\frac{m_1+m_2}{r^2} \\ &= -\frac{r^2}{a\,(1-e^2)}\left(\frac{df}{dt}\right)^2 \end{aligned} \tag{1.15}$$

Equation 1.12 becomes:

$$r\left(\frac{df}{dt}\right)^2\left[\frac{d^2\zeta}{df^2}+2j\frac{d\zeta}{df}\right]+\zeta\left[-\frac{r^2}{a\left(1-e^2\right)}\left(\frac{df}{dt}\right)^2\right]=-G\frac{m_1}{r^2r_1^3}\left(\zeta-\zeta_1\right)-G\frac{m_2}{r^2r_2^3}\left(\zeta-\zeta_2\right) \tag{1.16}$$

The non-dimensional position of the primaries still remains to be defined in order to have a precise expression for the distance of the spacecraft from them. As it is possible to deduce from Figure 1.2, the primaries lies on the x-axis, therefore they feature a null y value. By noting that the first primaries lies in the negative part of the x-axis, then it is possible to write:

$$\begin{aligned} x_1 &= -\frac{p_1}{1+e\cos(f)} \\ x_2 &= \frac{p_2}{1+e\cos(f)} \end{aligned}$$

It must be noted that the same eccentricity value appears in the previous expressions. The justification for this lies in the fact that it could be demonstrated that all the orbits described by the primaries features the same value of e: the orbit of P_1 around P_2, the one of P_2 around P_1 and, finally, those described by both the primaries about the center of mass of the system.

The values of each the semilatus-rectum, that is p_1 and p_2, is related to the eccentricity of the orbit of each primary around the center of mass of the system and to the semi-major axis of such orbit. Through some consideration about gravitational and centrifugal forces, as done by *Szebehely* [15], it is possible to reach the following result:

$$\frac{p_1}{p_2}=\frac{a_1}{a_2}=\frac{m_2}{m_1}$$

then se semi-major axes of P_1 orbit around the center of mass is $a_1=a\mu$, while for P_2 the result is $a_2=a\left(1-\mu\right)$. By recalling the definition of the semilatus-rectum $p=a\left(1-e^2\right)$, then the distances of the primaries from the center of mass become:

$$\begin{aligned} x_1 &= -\frac{a\mu\left(1-e^2\right)}{1+e\cos(f)} \\ x_2 &= \frac{a\left(1-\mu\right)\left(1-e^2\right)}{1+e\cos(f)} \end{aligned}$$

Now it is possible to obtain the non-dimensional form of the primaries position. It is sufficient to divide by the distance obtained in equation 1.6, thus resulting in:

$$\xi_1 = \frac{x_1}{r(f)} = -\mu \tag{1.17}$$

$$\xi_2 = \frac{x_2}{r(f)} = 1-\mu \tag{1.18}$$

Once obtained these result, by going back to eq. (1.16) is is possible to obtain the final form of the non-dimensional form of the equation of motion for the elliptic restricted three-body problem. There is still one more time derivative. It can be removed by dividing it by $r\left(\frac{df}{dt}\right)^2$. Doing so, the equation become:

$$\frac{d^2\zeta}{df^2} + 2j\frac{d\zeta}{df} = \frac{r}{a\left(1-e^2\right)}\left\{\zeta - \frac{a\left(1-e^2\right)}{r^2}\left(\frac{df}{dt}\right)^{-2}\left[-G\frac{m_1}{r^2 r_1^3}\left(\zeta-\zeta_1\right) - G\frac{m_2}{r^2 r_2^3}\left(\zeta-\zeta_2\right)\right]\right\}$$

The term multiplying the square brackets in the right-hand term is equivalent to:

$$\frac{r^2}{GM}$$

while the term outside the curly brackets can be rewritten in a form such that the true anomaly appears:

$$\frac{1}{1+e\cos(f)}$$

By splitting into the two components, which will be called ξ and η, and by finally expliciting the non-dimensional position of the primaries, the equations of motion are obtained:

$$\frac{d\xi^2}{df^2} - 2\frac{d\eta}{df} = \frac{1}{1+e\cos(f)}\left[\xi - \frac{1-\mu}{r_1^3}\left(\xi-\mu\right) - \frac{\mu}{r_2^3}\left(\xi+\mu-1\right)\right] \tag{1.19}$$

$$\frac{d\eta^2}{df^2} + 2\frac{d\xi}{df} = \frac{1}{1+e\cos(f)}\left[\eta - \frac{1-\mu}{r_1^3}\eta - \frac{\mu}{r_2^3}\eta\right] \tag{1.20}$$

with

$$r_1 = \sqrt{\left(\xi+\mu\right)^2+\eta^2} \tag{1.21}$$

$$r_2 = \sqrt{\left(\xi+\mu-1\right)^2+\eta^2} \tag{1.22}$$

It is possible to rewrite the right-hand term of eqs. (1.19) and (1.20) in terms of the spatial derivatives or, in case of the single equation with the imaginary unit

reported, the gradient of the so-called *force function* ω, which results from the ratio of the non-dimensional gravitational potential

$$\Omega = \frac{1}{2}\left(\xi^2 + \eta^2\right) + \frac{1-\mu}{r_1} + \frac{\mu}{r_2} + \frac{1}{2}\mu\left(1-\mu\right) \tag{1.23}$$

and the denominator of eq (1.6), therefore:

$$\omega = \frac{\Omega}{1 + e\cos(f)} \tag{1.24}$$

According to this results, the new form of eqs. (1.19) and (1.20) become:

$$\frac{d^2\zeta}{df^2} + 2j\frac{d\zeta}{df} = \nabla_\zeta \omega \qquad \text{or} \qquad \begin{aligned} \frac{d\xi^2}{df^2} - 2\frac{d\eta}{df} &= \frac{\partial\omega}{\partial\xi} \\ \frac{d\eta^2}{df^2} + 2\frac{d\xi}{df} &= \frac{\partial\omega}{\partial\eta} \end{aligned} \tag{1.25}$$

1.1.3 Polar Coordinates

As it can be observed from Figure 1.3 and Figure 1.4, a further representation of the problem is possible. According to this approach, a reference system centered in one of the primaries. Axes direction are selected such that the r-axis lies on the line joining the considered primary and the spacecraft, while the θ-axis is chosen perpendicular to r in the direction of increasing angle existing between the X-axis of the synodic reference frame and the x-axis of the polar reference frame. Hereafter both the P_2- and P_1-centered polar reference frames are presented.

To switch from the synodic reference frame to this new one, a translation of the origin and a rotation are necessary. Concerning the P_2-centered reference frame, starting from the spacecraft position vector:

$$\boldsymbol{r}_{syn} = \begin{bmatrix} 1 - \mu + r_2\cos(\theta_2) \\ r_2\sin(\theta_2) \end{bmatrix} \tag{1.26}$$

by setting the origin in P_2 it results

$$\boldsymbol{r}_{syn,P_2c} = \begin{bmatrix} r_2\cos(\theta_2) \\ r_2\sin(\theta_2) \end{bmatrix}$$

By eventually rotating about θ_2 with the following rotation matrix:

$$\boldsymbol{R}_{syn,P_2c\to r\theta,P_2c} = \begin{bmatrix} \cos(\theta_2) & \sin(\theta_2) \\ -\sin(\theta_2) & \cos(\theta_2) \end{bmatrix}$$

the position of the spacecraft within the r-θ, P_2-centered reference frame is obtained:

$$r_{r\theta,P_2c} = \begin{bmatrix} r_2 \\ 0 \end{bmatrix}$$

According to this definition, the new representation of the equation of motion can be obtained. Such topic is treated by *Topputo* e *Belbruno* [16]

$$r_2'' - r_2\theta_2'^2 - 2r_2\theta_2' = (1-\mu)\cos(\theta_2)\left(1 - \frac{1}{r_1^3}\right) + r_2\left(1 - \frac{1-\mu}{r_1^3}\right) - \frac{\mu}{r_2^3} \quad (1.27)$$

$$r_2\theta_2'' + 2r'\theta' - 2r_2' = (1-\mu)\sin(\theta_2)\left(\frac{1}{r_1^3} - 1\right) \quad (1.28)$$

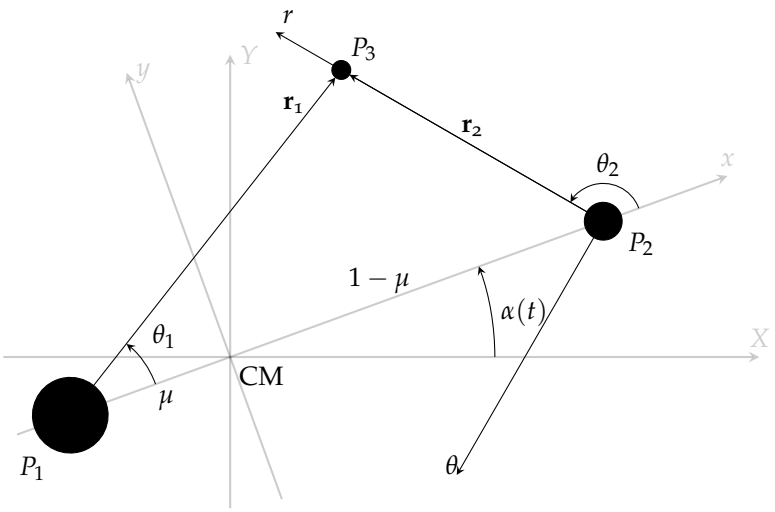

Figura 1.3: Polar P_2-centered reference frame

By applying an analogue reasoning it is possible to express the equations of motion in the polar, P_1-centered reference frame. The starting point is, once again, the spacecraft position vector expressed in equation 1.26, this time expressed with respect to θ_1. Therefore:

$$\boldsymbol{r}_{syn,P_1c} = \begin{bmatrix} r_1\cos(\theta_1) - \mu \\ r_1\sin(\theta_1) \end{bmatrix}$$

By eventually rotating about θ_1 with the following rotation matrix:

$$\boldsymbol{R}_{syn,P_1c\to r\theta,P_1c} = \begin{bmatrix} \cos(\theta_1) & \sin(\theta_1) \\ -\sin(\theta_1) & \cos(\theta_1) \end{bmatrix}$$

the position of the spacecraft within the r-θ, P_1-centered reference frame is obtained:

$$r_{r\theta,P_2c} = \begin{bmatrix} r_2 \\ 0 \end{bmatrix}$$

According to this definition, the new representation of the equation of motion can be obtained. The following representation is treated, once again, by *Topputo* e *Belbruno* [16]

$$r_1'' - r_1\theta_1'^2 - 2r_1\theta_1' = \mu\cos(\theta_2)\left(\frac{1}{r_2^3} - 1\right) + r_1\left(1 - \frac{1-\mu}{r_1^3}\right) - \frac{1-\mu}{r_1^3} \quad (1.29)$$

$$r_1\theta_1' + 2r_1'\theta_1' - 2r_1' = \mu\sin(\theta_2)\left(1 - \frac{1}{r_2^3}\right) \quad (1.30)$$

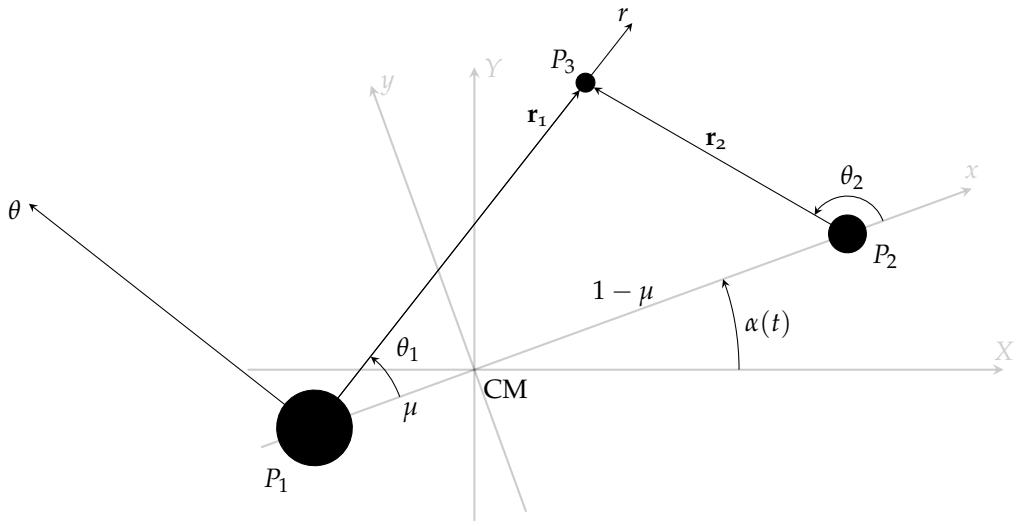

Figura 1.4: Polar P_1-centered reference frame

Handling the problem in polar coordinates allows to save time, since integration of the equations of motions is much quicker with respect to polar coordinates. Moreover, it is possible to retrieve directly the angle value (both θ_1 and θ_2). Of course there is much more interest in θ_2, due to the fact that interplanetary missions aim to reach the secondary primary of the system.

A more detailed analysis of the equations of motion in polar coordinates will be presented in the next chapter.

1.2 THE JACOBI CONSTANT

Just like the circular problem, even the elliptic one features an integral of motion. hereafter the retrieving procedure is illustrated. First of all, equations of motion reported in eqs. (1.19) and (1.20) are now recalled, but they will be rewritten in a more compact form for sake of simplicity. Accordingly, the derivative with respect to the true anomaly will be denoted with an apex and the derivative of the force function will be represented with a subscript. So:

$$\xi'' - 2\eta' = \omega_{/\xi} \tag{1.31}$$
$$\eta'' + 2\xi' = \omega_{/\eta} \tag{1.32}$$

For sake of completeness, the definition of the force function (and of the quantity related to it) is reported as well:

$$\omega = \frac{\Omega}{1 + e\cos(f)} = \frac{1}{1 + e\cos(f)} \left[\frac{1}{2}\left(\xi^2 + \eta^2\right) + \frac{1-\mu}{r_1} + \frac{\mu}{r_2} + \frac{1}{2}\mu\left(1-\mu\right) \right] \tag{1.33}$$

where the distance of the spacecraft from the primaries, r_1 and r_2, have been defined in equations 1.21 and 2.16 and are reported hereafter

$$r_1 = \sqrt{(\xi + \mu)^2 + \eta^2} \qquad \text{and} \qquad r_2 = \sqrt{(\xi + \mu - 1)^2 + \eta^2}$$

The next step consist in multiplying eq. (1.31) by ξ' and eq. (1.32) by η' and take the summation, thus obtaining:

$$\xi'\xi'' + \eta'\eta'' = \xi'\omega_{/\xi} + \eta'\omega_{/\eta} \tag{1.34}$$

It can be immediately noted that the right-hand term of eq. (1.34) is nothing but the derivative with respect to the true anomaly of the kinetic energy of the spacecraft. Concerning the right-hand term, its meaning can be deduced by applying the following reasoning. Knowing that the forcing function depends on ξ, η and f, by taking its derivative with respect to the true anomaly it results:

$$\frac{d\omega}{df} = \omega_{/\xi}\frac{d\xi}{df} + \omega_{/\eta}\frac{d\eta}{df} + \omega_{/f} \tag{1.35}$$

The first and the second elements of the right-hand term of equation 1.35 are exactly the starting point of this brief analysis, that is the right-hand term of eq. (1.34). Therefore such terms can be re-expressed as the difference of the ordinary and partial derivative of the forcing function with respect to the true anomaly. So far, eq. (1.34) has evolved into:

$$\frac{1}{2}\frac{d}{df}\left[\xi'^2+\eta'^2\right]=\frac{d\omega}{df}-\frac{\partial\omega}{\partial f} \tag{1.36}$$

At this stage, it is useful to express the partial derivative of the forcing function as:

$$\frac{\partial\omega}{\partial f}=\frac{e\Omega\sin(f)}{(1+e\cos(f))^2}$$

The very last step consist in integrating eq. (1.36) and isolating the kinetic energy integration constant. So:

$$\frac{1}{2}\left[\xi'^2+\eta'^2\right]+\frac{C}{2}=\omega-e\int\frac{\Omega\sin(f)}{(1+e\cos(f))^2}\,df \tag{1.37}$$

So, the expression of the Jacobi constant for the Elliptic Restricted Three-Body Problem is:

$$C=2\omega-\left(\xi'^2-\eta'^2\right)-2e\int\frac{\Omega\sin(f)}{(1+e\cos(f))^2}\,df \tag{1.38}$$

1.3 LAGRANGIAN POINTS

The concept of Lagrangian points is peculiar of the Three-Boby problem (both the circular and the elliptic). Such points identity the position where the combined gravitational pull of the primaries provides exactly the centripetal acceleration required to the spacecraft to orbit with them. In other words, a spacecraft located in a Lagrangian point is still with respect to both the primaries.

Being equilibrium points, then the spacecraft would experience null velocity and acceleration. Therefore, by setting to zero the left-hand term of eqs. (1.31) and (1.32), it result that their position is fully determined by:

$$\nabla\omega=0 \tag{1.39}$$

Recalling the definition of the force function (which is expressed in eq. (1.33) and noticing that the denominator $1+e\cos(f)$ never gets negative due to the fact that $e\in[0,1)$, the singularities of ω are exactly those of Ω.

Eq. (1.39) provides the following results:

$$\xi - \frac{(1-\mu)(\xi+\mu)}{r_1^3} - \frac{\mu(\xi-1+\mu)}{r_2^3} = 0 \tag{1.40}$$

$$\eta\left[1 - \frac{1-\mu}{r_1^3} - \frac{\mu}{r_2^3}\right] = 0 \tag{1.41}$$

where, once again, r_1 and r_2 are the distance of the spacecraft from the primaries and have been defined in eqs. (1.21) and (2.16). Starting from this results it is possible to note that two different kind of solutions are provided for $\eta = 0$ and for $\eta \neq 0$. The former make eq. (1.41) vanish. Therefore only eq. (1.40) needs to be evaluated. In this case three solutions are obtained. These points are called *collinear* due to the fact that they lie on the ξ-axis, two nearby the secondary primary and one behind the first one.

By labeling with l_i the distance of the i-th point from the closest primary, for the three collinears it is possible to perform a variable transformation between this distance and the location ξ of the same point in the synodic reference frame. Such relations are reported hereafter.

$$l_1 = (1-\mu) - \xi \tag{1.42}$$

$$l_2 = \xi - (1-\mu) \tag{1.43}$$

$$l_3 = -(\xi+\mu) \tag{1.44}$$

By inserting such expression into equation 1.40, three fifth-order polynomials are obtained:

$$l_1^5 - (3-\mu)l_1^4 + (3-2\mu)l_1^3 - \mu l_1^2 + 2l_1 - \mu = 0 \tag{1.45}$$

$$l_2^5 + (3-\mu)l_2^4 + (3-2\mu)l_2 s - \mu l_2^2 - 2\mu l_2 - \mu = 0 \tag{1.46}$$

$$l_3^5 + (2+\mu)l_3^4 + (1+2\mu)l_3^3 - (1-\mu)\left(l_3^2 - 2l_3 - 1\right) = 0 \tag{1.47}$$

According to *Jorba* e *Masdemont* [9], the system above is solved numerically by imposing the following initial conditions:

$$l_1^0 = \left(\frac{\mu}{3}\right)^{1/3} \qquad l_2^0 = \left(\frac{\mu}{3}\right)^{1/3} \qquad l_3^0 = 1 - \frac{7\mu}{12}$$

The second solution of eqs. (1.40) and (1.41) is obtained when, as already said, $\eta \neq 0$. The point located by this solutions are called *triangular* due to the fact that their distance from the primaries is identical. Their coordinate are:

$$\xi_{4,5} = \frac{1}{2} - \mu \tag{1.48}$$

$$\eta_{4,5} = \pm\frac{\sqrt{3}}{2} \tag{1.49}$$

The Lagrangian points map for the Sun-Mars system is reported in Figure 1.5. It must be noted that such map has been rescaled by a factor of 10^5 for sake of compactness of the representation

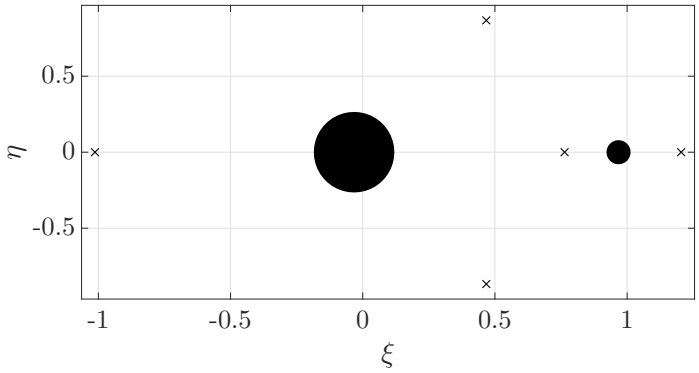

Figura 1.5: Re-scaled Lagrangian points map for the Sun-Mars system. The big circle represents the Sun, while the small one is Mars. Lagrangian points are marked with the $\times$ symbol.

1.4 PROXIMITY DYNAMICS: THE LEVI-CIVITA REGULARIZATION

A significant difference between the motion of celestial bodies and that of spacecrafts lies in the fact that close approach often occurs in the latter case, while in the former one is a very rare event. The consequence of this fact can be understood when the property of the gravitational force field is recalled, according to which the force acting between particles approach infinity when the distance between the bodies tends to zero. Therefore at collision (that is when r_1 or r_2 is zero) equations of motion, both in cartesian and polar form, feature singularities. However actual orbits never go through this points since, before this happens, their trajectory ends at the point of impact over the primary surface. However, by considering both the attractors and the spacecraft as point masses, collision can occur only at the singularity. From the computational point of view, such condition is of utmost importance.

Both the forces acting on the third body and its velocity increase as it gets closer to on of them. The stepsize of a numerical integration must be significantly reduced in order to retrieve reliable results. As consequence, integration will proceed very

slowly and, in the worst case, tolerance could not be respected, thus leading to the breaking of the integration itself. Despite these issues, singularities can be eliminated by proper re-definition of the maths related to the dynamics. Such modification of the problem is called *Levi-Civita regularization* and, within this work, it is performed only locally, that is nearby the primaries.

The regularization of the problem can be considered as a transformation of the dependent variable (ξ, η) into the new set (u, v). The aim of this process is to erase the singularities when r_1 and r_2 approach zero and, at the same time, provide a finite value of the velocity at the singularities. Moreover, it is worth considering a regularized dynamics in the region close to the primary, in fact computations are much quicker and results are precise as well.

In order to obtain the regularized dynamics of the spacecraft, the starting point is represented by the equations of motion written in the synodic reference frame (see eqs. (1.31) and (1.32)) and all the quantities related to the problem, in particular the force function (see eq. (1.33)) and the Jacobi constant (see eq. (1.38)). Following the procedure presented by *Szebehely* [15], by exploiting the complex notation both for the initial and final set of coordinate it results:

$$\boldsymbol{z} = \xi + j\eta \qquad \text{and} \qquad \boldsymbol{w} = u + jv \tag{1.50}$$

According to this new notation the equations of motion in compact form become:

$$\boldsymbol{z}'' + 2j\boldsymbol{z} = \nabla_z \omega \tag{1.51}$$

The transformation which realizes the regularization is a generic function $F(\boldsymbol{w})$ relating the original and the regularized variables, so that

$$\boldsymbol{z} = F(\boldsymbol{w})$$

Together with the coordinate transformation, also the independent variable in the initial framework, that is the true anomaly f, is changed into the new independent one in the new framework and it is labeled as τ. The relation between the old and the new independent variable is a function $g(\boldsymbol{w})$ such that:

$$\frac{df}{d\tau} = g(\boldsymbol{w})$$

The next step is to identify the relation existing between the F and the g functions. It is reported hereafter:

$$g(\boldsymbol{w}) = \left| \frac{F(\boldsymbol{w})}{d\boldsymbol{w}} \right|^2 \qquad \rightarrow \qquad \frac{df}{d\tau} = \left| \frac{F(\boldsymbol{w})}{d\boldsymbol{w}} \right|^2 \tag{1.52}$$

Thanks to the previous relation, it is possible to write the derivative of $\boldsymbol{z}$ with respect to f:

$$\boldsymbol{z}' = \frac{d\boldsymbol{z}}{d\boldsymbol{w}}\frac{d\boldsymbol{w}}{d\tau}\frac{d\tau}{df} = \frac{F(\boldsymbol{w})}{d\boldsymbol{w}}\frac{d\boldsymbol{w}}{d\tau}\left|\frac{d\boldsymbol{w}}{d\tau}\right|^{-2} = \frac{d\boldsymbol{w}}{d\tau}\left(\frac{\overline{dF}}{d\boldsymbol{w}}\right)^{-1} \tag{1.53}$$

where the barred term refers to the complex conjugated quantity. Using the Cauchy-Riemann relations the term on the right-hand side of eq.(1.51) can be related to the gradient in the new regularized framework (as done by *Szebehely* [15]):

$$\nabla_w \omega = \left(\frac{\overline{dF}}{d\boldsymbol{w}}\right)\nabla_z \omega \tag{1.54}$$

By taking the derivative of eq. (1.53), the last missing term to insert into eq. (1.51) is obtained, then they can be substituted in eq. (1.54); then isolating the second derivative of $\boldsymbol{w}$ the following expression is obtained:

$$\frac{d^2\boldsymbol{w}}{d\tau^2} + 2j\frac{d\boldsymbol{w}}{d\tau}\left|\frac{dF}{\boldsymbol{w}}\right|^2 = \left|\frac{dF}{d\boldsymbol{w}}\right|^2\nabla_w V + \left|\frac{d\boldsymbol{w}}{d\tau}\right|^2\frac{\overline{d^2F}}{d\boldsymbol{w}^2}\left(\frac{\overline{dF}}{d\boldsymbol{w}}\right)^{-1} \tag{1.55}$$

where the term V is given by:

$$V = \omega - \frac{1}{2}C$$

This can be done because C is constant, so $\nabla V \equiv \nabla\omega$. From the expression of the Jacobi constant (see eq. 1.38), the velocity can be extracted and written as:

$$|\boldsymbol{z}'|^2 = \left|\frac{d\boldsymbol{z}}{df}\right|^2 = \left(x'^2 + y'^2\right) = 2\left(V - I\right) \tag{1.56}$$

where I correspond, for sake of simplicity, to

$$I = e\int \frac{\Omega\sin(f)}{\left(1 + e\cos(f)\right)^2}df \tag{1.57}$$

By substituting the expression of $\boldsymbol{z}$ obtained in eq. (1.53) into eq. (1.56), an expression for the norm of the velocity in the regularized equations is found:

$$\left|\frac{d\boldsymbol{w}}{d\tau}\right| = 2\left|\frac{dF}{d\boldsymbol{w}}\right|^2\left(V - I\right) \tag{1.58}$$

By substituting this last relation into eq. (1.55), the regularized equations of motion (in complex notation)are obtained:

$$\frac{d^2\boldsymbol{w}}{d\tau^2} + 2j\frac{d\boldsymbol{w}}{d\tau}\left|\frac{dF}{\boldsymbol{w}}\right|^2 = \nabla_w\left(V\left|\frac{dF}{d\boldsymbol{w}}\right|^2\right) - 2I\frac{dF}{d\boldsymbol{w}}\overline{\frac{d^2F}{d\boldsymbol{w}^2}} \tag{1.59}$$

Once the equations for the regularized system are obtained, the transformation $F(\boldsymbol{w})$ remains to be defined. Since the regularization is performed *locally*, then two different transformation will be considered, each one removing the singularity nearby the i-th primary. Therefore

$$\text{Nearby } P_1\text{:}\quad F_1(\boldsymbol{w}) = \boldsymbol{w}^2 - \mu \quad \rightarrow \quad \begin{cases} \xi = u^2 - v^2 - \mu \\ \eta = 2uv \end{cases} \tag{1.60}$$

$$\text{Nearby } P_2\text{:}\quad F_2(\boldsymbol{w}) = \boldsymbol{w}^2 + (1-\mu) \quad \rightarrow \quad \begin{cases} \xi = u^2 - v^2 + (1-\mu) \\ \eta = 2uv \end{cases} \tag{1.61}$$

From these relations, the transformations from (ξ, η) to (u, v) are obtained:

$$\text{Nearby } P_1\text{:} \qquad \begin{cases} u^2 = \dfrac{\xi+\mu}{2} \pm \sqrt{\dfrac{(\xi+\mu)^2}{4} + \dfrac{\eta^2}{4}} \\ v = \dfrac{\eta}{2u} \end{cases} \tag{1.62}$$

$$\text{Nearby } P_2\text{:} \qquad \begin{cases} u^2 = \dfrac{\xi-1+\mu}{2} \pm \sqrt{\dfrac{(\xi-1+\mu)^2}{4} + \dfrac{\eta^2}{4}} \\ v = \dfrac{\eta}{2u} \end{cases} \tag{1.63}$$

In both cases, two solution for u and v are admitted. By naming

$$\begin{aligned} r_{1x} &= \xi + \mu \\ r_{2x} &= \xi - 1 + \mu \end{aligned}$$

it can be noted that

$$\begin{aligned} r_1^2 &= r_{1x}^2 + \eta^2 \\ r_2^2 &= r_{2x}^2 + \eta^2 \end{aligned}$$

In general the solution providing real values for u and v is preferred. Accordingly the expression with the plus sign for u are chosen in eqs. (1.62) and (1.63) (usually it is $r_i > r_{ix}$). Therefore:

$$\text{Nearby } P_1: \quad \begin{cases} u = \sqrt{\frac{1}{2}(r_1 + r_{1x})} \\ v = \frac{\eta}{2u} \end{cases} \tag{1.64}$$

$$\text{Nearby } P_2: \quad \begin{cases} u = \sqrt{\frac{1}{2}(r_2 + r_{2x})} \\ v = \frac{\eta}{2u} \end{cases} \tag{1.65}$$

According to this transformation, the distance from the primaries become:

$$\text{Nearby } P_1: \quad \begin{cases} r_1 = (u^2 + v^2) \\ r_2 = \sqrt{(u^2 + v^2) - 2(u^2 - v^2) + 1} \end{cases} \tag{1.66}$$

$$\text{Nearby } P_2: \quad \begin{cases} r_1 = \sqrt{(u^2 + v^2) + 2(u^2 - v^2) + 1} \\ r_2 = (u^2 + v^2) \end{cases} \tag{1.67}$$

Referring again to eqs. (1.64) and (1.65), it can be noted that u and v have singularities when $y = 0$ and, at the same time, $r_{ix} < 0$. In this case, in fact, $|r_i| = |r_{ix}|$ and u results to be zero having as consequence an undefined value for v. This is equivalent to have the third particle within the so called *Levi-Civita circle* with an angle exactly equal to $\theta_i = \pi$, hence this event occurs only if initial conditions are chosen with $r_i < r_{LC}$ and $\theta_i = \pi$. Therefore, in order not to have this kind of problem, it is sufficient to select a different initial condition.

The next step is to obtain the expression for the regularized velocity. Recalling the definition of $\mathbf{z}'$ (which is reported in eq. 1.53) the transformation from (ξ', η') to (u', v') are obtained:

$$\xi' = \frac{uu' - vv'}{2(u^2 + v^2)} \tag{1.68}$$

$$\eta' = \frac{uu' + vv'}{2(u^2 + v^2)} \tag{1.69}$$

by inverting these relations:

$$u' = 2u\xi' + 2v\eta' \tag{1.70}$$

$$v' = 2u\eta' - 2v\xi' \tag{1.71}$$

It must be noted that these last relations are the same for both regularizations around P_1 and P_2 because $\mathbf{z}'$ contains only $dF/d\boldsymbol{w} = 2\boldsymbol{w}$, which is the same for both the cases.

At this point, the equations of motion will be obtained for the regularized plane both around P_1 and P_2. The starting point is the following system:

$$u'' - 8v'\left(u^2+v^2\right) = \frac{\partial}{\partial u}\left[4V_i\left(u^2+v^2\right)\right] - 8uI \tag{1.72}$$

$$v'' + 8u'\left(u^2+v^2\right) = \frac{\partial}{\partial v}\left[4V_i\left(u^2+v^2\right)\right] - 8vI \tag{1.73}$$

where the differences between the two cases are all contained in the term $V_i = \omega - C_2$. According to the considered primary, a different expression appears. So nearby P_1:

$$\begin{aligned} V_1 = \frac{1}{1+e\cos(f)}\Bigg\{\frac{1}{2}\left[\left(u^2+v^2\right)^2 - 2\mu\left(u^2-v^2\right)+\mu^2\right] \\ + \frac{1+\mu}{r_1} + \frac{\mu}{r_2} + \frac{1}{2}\mu\left(1-\mu\right)\Bigg\} - \frac{C}{2} \end{aligned} \tag{1.74}$$

with r_1 and r_2 defined in eq. (1.66). On the other hand nearby P_2:

$$\begin{aligned} V_2 = \frac{1}{1+e\cos(f)}\Bigg\{\frac{1}{2}\left[\left(u^2+v^2\right)^2 - 2\left(1-\mu\right)\left(u^2-v^2\right)+\left(1-\mu\right)^2\right] \\ + \frac{1+\mu}{r_1} + \frac{\mu}{r_2} + \frac{1}{2}\mu\left(1-\mu\right)\Bigg\} - \frac{C}{2} \end{aligned} \tag{1.75}$$

with r_1 and r_2 defined in eq. (1.67). It must be remarked that within eqs. (1.72) and (1.73), the function V_i is multiplied by a term which comes from the derivative of the transformation function $F_i(\boldsymbol{w})$ with respect to the complex variable $\boldsymbol{w}$

$$\left|\frac{dF_i(\boldsymbol{w})}{d\boldsymbol{w}}\right| = |2\boldsymbol{w}| = 4\left(u^2+v^2\right)$$

The product of this term with V_1 and V_2 deletes the terms $1/r_1$ and $1/r_2$, respectively, which causes the singularities in the equations of motion. Calculating the derivatives of these products with respect to the regularized variables (u, v), the last terms still not known in eqs. (1.72) and (1.73) are obtained. First the regularization nearby P_1:

$$\begin{aligned}\frac{\partial}{\partial u}\left[4\left(u^2+v^2\right)V_1\right] &= \frac{1}{1+e\cos(f)}\left\{12u\left(u^2+v^2\right)^2-16\mu u^3+\right.\\ &+4\mu^2u+8u\frac{\mu}{r_2}+4\mu u\left(1-\mu\right)\\ &\left.-8u\frac{\mu}{r_2^3}\left(u^2+v^2\right)\left[\left(u^2+v^2\right)-1\right]\right\}-4Cu \quad (1.76)\\ \frac{\partial}{\partial v}\left[4\left(u^2+v^2\right)V_1\right] &= \frac{1}{1+e\cos(f)}\left\{12v\left(u^2+v^2\right)^2-16\mu v^3+\right.\\ &+4\mu^2v+8v\frac{\mu}{r_2}+4\mu v\left(1-\mu\right)\\ &\left.-8v\frac{\mu}{r_2^3}\left(u^2+v^2\right)\left[\left(u^2+v^2\right)-1\right]\right\}-4Cv \quad (1.77)\end{aligned}$$

The same operations can be performed nearby P_2, thus producing:

$$\begin{aligned}\frac{\partial}{\partial u}\left[4\left(u^2+v^2\right)V_2\right] &= \frac{1}{1+e\cos(f)}\left\{12u\left(u^2+v^2\right)^2-16\left(1-\mu\right)u^3+\right.\\ &+4\left(1-\mu\right)^2u+8u\frac{1-\mu}{r_1}+4\mu u\left(1-\mu\right)\\ &\left.-8u\frac{1-\mu}{r_1^3}\left(u^2+v^2\right)\left[\left(u^2+v^2\right)-1\right]\right\}-4Cu \quad (1.78)\\ \frac{\partial}{\partial v}\left[4\left(u^2+v^2\right)V_2\right] &= \frac{1}{1+e\cos(f)}\left\{12v\left(u^2+v^2\right)^2-16\left(1-\mu\right)v^3+\right.\\ &+4\left(1-\mu\right)^2v+8v\frac{1-\mu}{r_1}+4\mu v\left(1-\mu\right)\\ &\left.-8v\frac{1-\mu}{r_1^3}\left(u^2+v^2\right)\left[\left(u^2+v^2\right)-1\right]\right\}-4Cv \quad (1.79)\end{aligned}$$

By inserting these expression into eqs. (1.72) and (1.73), the complete form of the regularized equations of motion can be obtained. Eventually, the presence of the true anomaly must be briefly discussed: in the regularized plane, f represent nothing but the independent variable, then it is obtained by integrating also the relations between it and τ. This expression can be written as follows:

$$\frac{df}{d\tau}=\left|\frac{F(\boldsymbol{w})}{d\boldsymbol{w}}\right|^2 \qquad \rightarrow \qquad f'=4\left(u^2+v^2\right) \quad (1.80)$$

As in can be noted, this equation can be integrated together with the equations written before, thus providing as initial conditions the true anomaly in which the

third particle enters the Levi-Civita circle. Similarly, the integral I (defined in eq. (1.57)) must be analyzed. By re-writing it in as function of τ, the following is obtained:

$$I = e \int \frac{\Omega \sin(f)}{(1 + e\cos(f))^2} 4 \left(u^2 + v^2\right) d\tau \tag{1.81}$$

By taking the derivative with respect to τ:

$$I' = \frac{dI}{d\tau} = e \frac{\Omega \sin(f)}{(1 + e\cos(f))^2} 4 \left(u^2 + v^2\right) \tag{1.82}$$

By integrating this expression step by step, the value of I to insert into the regularized equations of motion is obtained. When entering the Levi-Civita circle, the initial conditions for I' cam be obtained by inverting the expression of the Jacobi constant C

$$I = \omega - \frac{1}{2}\left(\xi'^2 + \eta'^2\right) - \frac{C}{2} \tag{1.83}$$

where C is obtained from the same expression, evaluated at the initial instant $f = f_0$ (or $\tau = \tau_0$): in this case, in fact, the integral term is null by definition.

2 THE WEAK STABILITY BOUNDARY

In this chapter the technique used to search a class of special trajectory will be introduced. During the last years one of the most studied methods applies the definition of the so called weak stability boundaries (WSB) which, roughly speaking, can be seen as the boundary of a region near the target planet where the capture of the third particle occurs. Across the boundary of this regions the influence of the bigger primary is relevant and for th reason the WSB are also considered as transition regions. This technique developed at the end of the 80s by E. A. Belbruno and J. K. Miller, was successfully applied in October 1991 to save the Japanese satellite Hiten; which was able to reach the Moon. In the following sections a detailed definition of the weak stability boundary will be given first, then, the problems involved in their calculation will be faced.

2.1 BALLISTIC CAPTURE

In order to have a complete understanding of the weak stability boundaries, it is necessary to explain another fundamental concept strictly connected with them: the definition of *ballistic capture*. Extending to a general case the description given in [14], it is possible to say that ballistic capture by planet occurs when an object (for example a satellite) enters, under natural dynamics, within the sphere of influence of that planet and makes at least one complete revolution around it. The expression *under natural dynamics* means that, in order to revolve around the planet, no further energy must be provided to the object. If ballistic capture does not occur, the energy difference that is necessary to obtain the capture, must be furnished with other means, e.g. by maneuvering the satellite thus using propellant. Thanks to the ballistic capture, the use of propellant is avoided and the saved mass can be used for other maneuvers (if necessary) or assigned to other subsystems during the mission design. For this reason, this kind of solutions can be called *low-cost* transfers. Usually they are also named *low-energy* transfers because in general their energetic level is considerably lower than the ne of the trajectories obtained with the typical *patched conics* approach. The basic idea of WSB has been first illustrated by E. A. Belbruno K. Miller in two important papers (*Belbruno* e *Miller* [3] and *Miller* e *Belbruno* [14]), then resumed by *Belbruno* [1]; furthermore other detailed explications can be found in *Belbruno*, *Gidea* e *Topputo* [2], *Circi* e *Teofilatto* [4] and *García* e *Gómez* [6]. Differently from the just cited bibliography, in this thesis a definition of Weak stability boundaries is showed but, publications, the Kepler energy of the third particle in a reference system referred to the smaller primary must be coordinate system is represented in Figure 2.1, where the couple (X_{II}, Y_{II}) represents the sidereal axes centered in P_2.

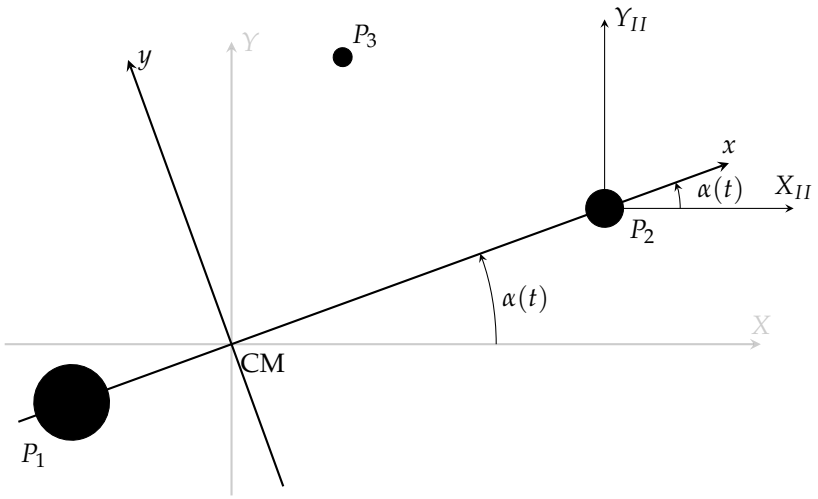

Figura 2.1: Sidereal reference frame centered in P_2.

The Kepler energy expression is the following:

$$H_2 = \frac{1}{2}v^2 - \frac{\mu}{r_2} \tag{2.1}$$

As it can be seen, the typical mass parameter of the two body problem, k, is substituted by the (dimensionless) mass parameter μ, while the velocity v is referred to the inertial reference system centered in P_2. If the solution of the elliptic restricted three-body problem is indicated using the flow of system $\phi(f)$:

$$\phi(f) = \left(X_{II}, X'_{II}\right)$$

It is possible to define ballistic capture in a formal way for the ERTBP, where the independent variable is the true anomaly f (related to the time through the Kepler equation, as explained in the previous chapter). In this case in fact from the energetic point of view the following events can be identified

- *Ballistic capture at* P_2: it occurs at anomaly f_1 if $H_2(\phi(f_1)) \leq 0$
- *Temporary ballistic capture at* P_2: if $H_2(\phi(f)) \leq 0$ for $f_1 \leq f \leq f_2$ and $H_2(\phi(f)) > 0$ for $f < f_1$ and for $f > f_2$, with finite values of f_1, f_2 and $f_1 < f_2$
- *Ballistic ejection (escape) from* P_2: it happens at f_1 if, for $f < f_1$, $H_2(\phi(f_1)) \leq 0$ and for $f \geq f_1$, $H_2(\phi(f_1)) > 0$

Note that these definitions are formally the same as those given in literature (*Belbruno* [1], *Belbruno*, *Gidea* e *Topputo* [2], *Topputo* e *Belbruno* [16]), with the only difference that the time is substituted by the true anomaly; they can also be applied to the biggest primary P_1 if the energy relative to a reference system centered on it is considered. If

the independent variable is decreasing, the definition of ballistic capture remains the same, being it a punctual property of P_3, while the definition of temporary ballistic capture and ballistic ejection can be anyway stated, but applying small variations to the previous definitions:

- Backward temporary ballistic capture at P_2: if $H_2(\phi(f)) \leq 0$ for $f_2 \leq f \leq f_1$ and $H_2(\phi(f)) > 0$ for $f > f_1$ and for $f < f_2$, with the finite values of f_1, f_2 and $f_1 > f_2$;
- Backward ballistic ejection (escape) from P_2: it happens at f_1 if for $f > f_1$, $H_2(\phi(f)) < 0$ and for $f \leq f_1$, $H_2(\phi(f)) \geq 0$.

To define the regions in which ballistic capture can occur, together with the .just cited energetic aspects, also geometrical considerations concerning the trajectory of P_3 must be stated: in fact only after a definition of the geometrical requirements of ballistic capture to occur, it will be possible to complete the definition of WSB, as explained in the following section.

2.2 DEFINITION OF WEAK STABILITY BOUNDARY

If the ballistic capture at P_2 has to be verified, the revolutions of the third particle around the smaller primary have to be tracked; for this reasons only trajectories with the following characteristics will be studied (*Belbruno* [1], *Szebehely* [15]) see also Figure 2.2

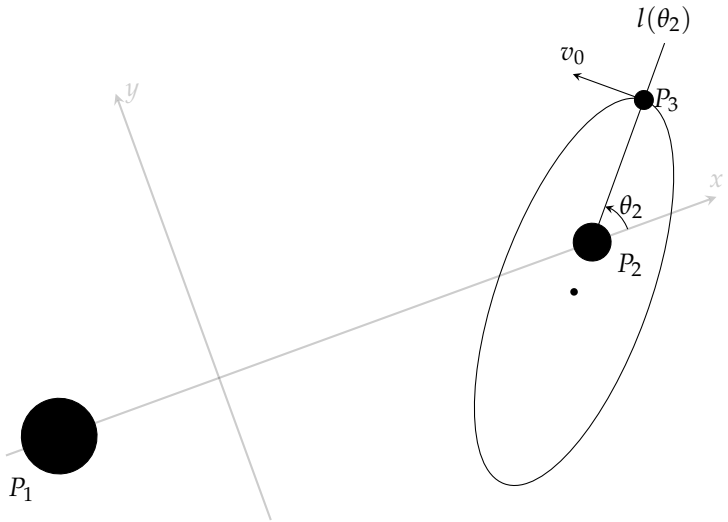

Figura 2.2: Initial velocity and related elliptic orbit around P_2

1. The initial position of the third particle is on the radial Segment $l(\theta_2)$ departing from P_2 and making an angle θ_2 with the x-axis of the synodic dimensionless

reference system. This starting point of the third particle is considered to be the *periapsis* of an initial elliptic orbit with fixed eccentricity $0 \leq e < 1$ and whose semi-major axis lies on the line $l(\theta_2)$. Hence calling a the dimensionless semi-major axis, the initial distance from P_2 is given by $r_2 = a(1-e)$.

2. Being on the periapsis of an elliptic orbit, the initial velocity, whose magnitude is obtained from the solution of the two body problem, will be normal to the line $l(\theta_2)$. Once the parameters e and θ_2 are chosen, the initial velocity depends only on the initial distance r_2 and on the direction of the initial velocity, which can be chosen to be prograde (counterclockwise) or retrograde (clockwise). Thanks to this definition of the initial state of P_3, the initial energy is always $H_2(\phi(f_0)) < 0$.

3. After evaluating the initial state, the equations of the ER3BP can be integrated and, according to the definition of ballistic capture, the motion is said to be n-stable if the third particle, without making any revolutions around P_1, makes n turns around P_2, returning after each turn on a point belonging to the line $l(\theta_2)$ with negative Kepler energy H_2; otherwise the motion is said to be *n-unstable* (see Figure 2.3)

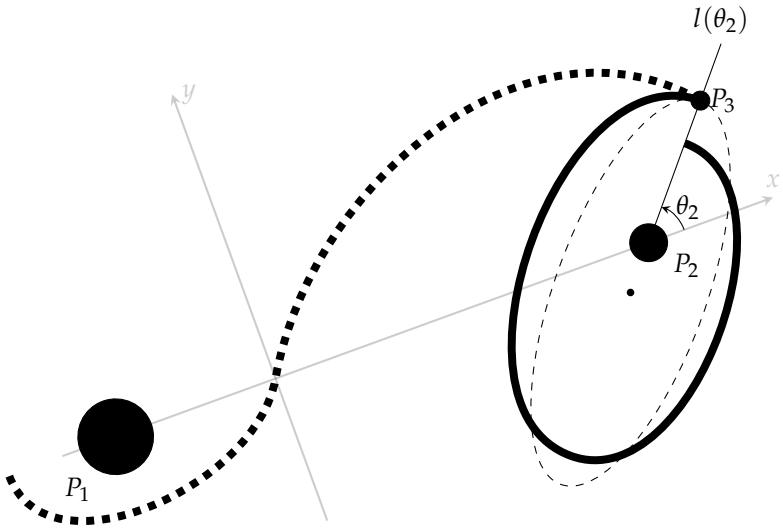

Figura 2.3: Possible trajectories given the initial velocity v_0. The full thick line represent an acceptable trajectory (note the decreasing of H_2 producing an altitude reduction), while the dashed thick line depicts a non acceptable path due to the fact that a revolution about P_1 is performed.

The third point above does not state when a condition is considered unstable: this can occur either if the third particle makes at least one revolution around the other primary P_1 (then a primary interchange escape occurs), or if the particle completes the desired number of turns around P_2, but it arrives on the line $l(\theta_2)$ with a positive

Kepler energy. Another possibility can happen: for some initial conditions in fact the third particle does not perform any revolution neither around P_1 nor around P_2; although these situations are not formally unstable, they cannot be considered stable and for this reason they are classified as unstable conditions.

In the three points listed above the eccentricity e of the initial elliptic orbit of P_3 around P_2 is mentioned. It must be remarked that this value must not be confused with the eccentricity of the orbit of the second primary around P_1, for this reason this last eccentricity, typical of the ER3BP, will be labeled e_p from now on.

Using the definitions given above and fixing the initial values of r_2 and θ_2, it is possible to check whether the corresponding initial state brings to ballistic capture or not; then applying the same procedure to a set of different θ_2 and r_2 (but the same eccentricity of the initial ellipse), the corresponding stable conditions can be found, thus defining an entire n-stable set.

Usually only n-stable sets with $n \geq 1$ have been considered in literature; thanks to the definition given before of ballistic capture in the case of decreasing anomaly, it is now possible to define also a *negative stable sets*, that is with $n \leq -1$. The three points listed before in fact do not involve the independent variable, extending their validity also when backward integration of the equations of motion is performed. This possibility, still never exploited when studying weak stability boundaries, will be an important element in finding the desired trajectories, as illustrated in the following chapters.

2.3 WEAK STABILITY BOUNDARY AS CONTOUR OF A STABLE SET

Once the stable sets are defined, it can happen that point close to P_2 are stable, then moving on the same line $l(\theta_2)$, but for higher values of initial distance r_2, some unstable points are found and finally, for still higher value of r_2 the relative initial conditions return to be stable again. Thus, in general, a n-stable set is defined as the union of open intervals containing the single subset of stable initial conditions.

$$\mathcal{W}_n\left(\theta_2, e, f_0\right) = \bigcup_{k \geq 1} \left(r^*_{2k-1}, r^*_{2k}\right) \tag{2.2}$$

Here the points of the type r^*, located at the the beginning and at the end of every interval, represent the unstable point delimiting each stable subset. The just defined set contains all the stable conditions along the line $l(\theta_2)$ for a fixed value of θ_2, e and f_0: being the ER3BP a *non-autonomous* problem, the equations of motion produce different solutions if different intervals of independent variable f are considered, hence the initial value of the true anomaly must be also specified. If the same sets are

then obtained for each value of θ_2, the complete set (for fixed e and f_0) is given by:

$$\mathcal{W}_n(f_0) = \bigcup_{\theta_2 \in [0,2\pi)} \mathcal{W}_n(\theta_2, e, f_0) \tag{2.3}$$

Finally if different sets$\mathcal{W}_n(, e, f_0)$ are computed, each one for a fixed value of eccentricity e, the open stable set is obtained as follows:

$$\mathcal{W}_n(f_0) = \bigcup_{e \in [0,1)} \mathcal{W}_n(e, f_0) \tag{2.4}$$

It must be remarked that every set $\mathcal{W}_n(\theta_2, e, f_0)$, $\mathcal{W}_n(e, f_0)$ and $\mathcal{W}_n(f_0)$ is an *open* set. After the formal definition of the stable sets, the Weak Stability Boundary can be defined using the same procedure of [3, 22]:

The *Weak Stability Boundary* of order n, called $\partial\mathcal{W}_n(f_0)$, is the locus of points $r^*(\theta_2, e)$ along the radial segment $l(\theta_2)$ in which there is a change of stability of the trajectory of the third particle; then $r^*(\theta_2, e)$ represents one of the generic extreme points of each interval (r^*_{2k-1}, r^*_{2k}), where every $r_2 \in (r^*_{2k-1}, r^*_{2k})$ gives a n-stable trajectories and there exist $r_2^{'}(r^*_{2k-1}, r^*_{2k})$ arbitrarily close to r^*_{2k-1} or r^*_{2k} which produce n-unstable trajectories.

Thus the definition of WSB can be formally expressed as:

$$\partial\mathcal{W}_n(f_0) = \{r^*(\theta_2, e) \,|\theta_2 \in [0, 2\pi], e \in [0, 1]\} \tag{2.5}$$

Now it is clear why the generic $\partial\mathcal{W}_n(f_0)$ is considered the boundary of the relative n-stable set $\mathcal{W}_n(f_0)$. As can be noticed, both $\partial\mathcal{W}_n(f_0)$ and $\mathcal{W}_n(f_0)$ can be represented in a three dimensional space, where each point corresponds to a precise value for the elements (e, θ_2, r_2).

2.4 SOME CONSIDERATIONS ABOUT THE COMPUTATION OF STABLE SETS

In the previous section, n-stable sets and weak stability boundaries have been defined. According to such definitions in can be understood that, if the WSB are desired, the most problematic passage in the whole procedure is not the calculation of the WSB itself, but the calculation of the stable set. Once the eccentricity e has been fixed and the initial angle θ_2 has been chosen, every single point r_2 lying on the line $l(\theta_2)$ gives the initial conditions (r_2, v), where the initial velocity is normal to the line $l(\theta_2)$, as explained in the previous section; remembering also that $H_2 = -\mu/2a$,

its modulus can be evaluated starting from the expression of the Kepler energy given in eq. (2.1), so that:

$$v = \sqrt{\mu \frac{1+e}{r_2}} \tag{2.6}$$

Remarking that the pair (r_2, v) is relative to the *sidereal* reference frame centered in P_2, the initial conditions must be transformed in the synodic baricentric reference frame, in coherence with equations of motions reported in the previous chapter. By looking at Figure 2.2, the position in the synodic coordinates can be immediately obtained remembering that P_2 is located at $1-\mu$. Then, for the spacecraft it follows that:

$$\begin{aligned} \xi &= 1-\mu+r_2\cos(\theta_2) && (2.7)\\ \eta &= r_2\sin(\theta) && (2.8) \end{aligned}$$

The velocity must be transformed too. In this case its modulus is given by eq. (2.6),however to obtain the components within the synodic reference frame, the terms due to the angular velocity of this last reference system must be subtracted [1], so that:

$$\begin{aligned} \xi' &= -v\sin(\theta_2)+r_2\sin(\theta_2) && (2.9)\\ \eta' &= v\cos(\theta_2)-r_2\cos(\theta_2) && (2.10) \end{aligned}$$

Having the initial conditions, the equations of the elliptic problem, recalled from the first chapter can be solved:

$$\begin{aligned} \xi'' - 2\eta' &= \omega_{/\xi}\\ \eta'' + 2\xi' &= \omega_{/\eta} \end{aligned}$$

with:

$$\omega = \frac{\Omega}{1+e\cos(f)} = \frac{1}{1+e\cos(f)}\left[\frac{1}{2}\left(\xi^2+\eta^2\right)+\frac{1-\mu}{r_1}+\frac{\mu}{r_2}+\frac{1}{2}\mu\left(1-\mu\right)\right]$$

and:

$$\begin{aligned} r_1 &= \sqrt{(\xi+\mu)^2+\eta^2}\\ r_2 &= \sqrt{(\xi+\mu-1)^2+\eta^2} \end{aligned}$$

[1] This angular velocity is formally α', but being $\alpha = f+\bar{\omega}$ as defined in the first chapter, it results that $\alpha' = 1$.

When trying to solve this system, some practical problems appear: first of all, it becomes necessary to set a limit value of the independent variable for the integration, hence a *true anomaly limit*, f_{lim}. Doing so, the integration of the equations of motion must continue until f_{lim} is reached. The choice of the limit value is of utmost importance: it must be high enough (or small enough for backward integration) to allow the assessment of every initial conditions, without breaking the integration before a possible ballistic capture would occur. The drawback of this approach of this approach is that while a higher value for the anomaly limit is necessary for the motivation just explained, choosing it quite high implies at the same time the integration the equations of motion for long anomaly intervals, thus needing an excessive computational time [2]. Hence the true anomaly limit should be a compromise between these two contrasting aspects. A possible solutions could be the evaluation of the angle θ_2 for every integration step. Doing so the integrations could be interrupted when the desired revolutions around P_2 occur; the problem is that, unfortunately, using the common integrators built-in in Matlab, the necessary calculations of the involved angle cannot be performed during every integration step[3] and the development of an integrator *ad hoc* for the elliptic problem is not the intent of this thesis. For this reason the solution to this problem can be obtained only if the angle θ_2 is given directly by the integrator; hence, following what done in "Computation of weak stability boundaries: Sun–Jupiter system", it has been chosen to solve the equations of motion directly in polar coordinates. Another problem existing either in polar and cartesian coordinates is represented by the singularities of the equations of motion. As already mentioned in the previous chapter, the equations of motion become undefinied if $r_1 = 0$ or $r_2 = 0$. In this thesis, in order to solve this problem, a *local regularitazion* is performed when the spacecraft flies nearby a primary. The regularization method is applied to the synodic cartesian reference frame, where the problem of the limit value on the true anomaly is still present, but in this case it involves a small subset of initial conditions, as will be explained in the following sections, after a description of the equations in polar coordinates.

2.5 EQUATIONS OF MOTION IN POLAR COORDINATES

For the motivations discussed before, it has been chosen to solve the equations of motion in polar coordinates: doing so the angle θ_2 is directly computed, thus giving the possibility to verify through this angle if the desired turns of the spacecraft about P_2 are completed. Before applying the transformation of coordinates it is useful to recall the equations of motion in compact form:

$$\xi'' - 2\eta' = \omega_{/\xi} \tag{2.11}$$
$$\eta'' + 2\xi' = \omega_{/\eta} \tag{2.12}$$

[2] Normally some hundreds of thousands of initial conditions must be checked

[3] To obtain the angle θ_2 from the pair (x, y), the trigonometric inverse functions must be used and they are, as well known, non-continuous functions.

or in vector notation:

$$\boldsymbol{\xi}'' + 2\boldsymbol{\omega} \times \boldsymbol{\xi}' = \boldsymbol{\nabla}\omega \tag{2.13}$$

where the second element of the left-hand side represents the Coriolis accelerations. The quantity $\underline{\omega}$ (not to be confused with the force function) is in fact the *non-dimesional* angular velocity of the baricentric synodic reference frame defined by the two primaries. In other words: $\boldsymbol{\omega} = \alpha'(f)\hat{\boldsymbol{k}}$. As mentioned in the previous section, the equations in circular coordinates centered in P_2 are desired. In this last reference frame, the pair of dependent variables is given hy (r_2, θ_2). To perform the transformation, two different methods are available: the first exploits the relation existing between the old variables (ξ, η) and the new ones (r_2, θ_2), thus giving:

$$\xi = 1 - \mu + r_2 \cos(\theta_2) \tag{2.14}$$
$$\eta = r_2 \sin(\theta_2) \tag{2.15}$$

If these expressions and their derivatives with respect to the true anomaly are substituted in the equations of motion, two equations are obtained, both containing the terms r_2'' and θ_2''; then a combination of them must be found in order to have two independent equations, on for r_2'' and another for θ_2''.

The other way to obtain the transformed equations uses first a change of the origin of the synodic reference frame, which is moved from the pericenter to P_2; then a rotation about the $\hat{\mathbf{k}}$-axis is applied (this axis in the polar reference frame remains parallel to the original one). The rotation is governed by the following relations:

$$\hat{\boldsymbol{r}}_2 = \cos(\theta_2)\hat{\boldsymbol{i}} + \sin(\theta_2)\hat{\boldsymbol{j}} \tag{2.16}$$
$$\hat{\boldsymbol{\theta}}_2 = -\sin(\theta_2)\hat{\boldsymbol{i}} + \cos(\theta_2)\hat{\boldsymbol{j}} \tag{2.17}$$

here the couple $(\hat{\boldsymbol{i}}, \hat{\boldsymbol{j}})$ represents the unit vectors of the synodic reference frame. By deriving these last equations with respect to the true anomaly, the velocity and the acceleration of the new unit vectors can be obtained:

$$\hat{\mathbf{r}}_2' = \theta_2'\hat{\boldsymbol{\theta}}_2 \tag{2.18}$$
$$\hat{\boldsymbol{\theta}}_2' = -\theta_2'\hat{\boldsymbol{r}}_2' \tag{2.19}$$

and

$$\hat{\boldsymbol{r}}_2'' = -\theta_2'^2\hat{\boldsymbol{r}}_2' + \theta_2''\hat{\boldsymbol{\theta}}_2 \tag{2.20}$$
$$\hat{\boldsymbol{\theta}}_2'' = -\theta_2''\hat{\boldsymbol{r}}_2 - \hat{\boldsymbol{r}}_2'^2\hat{\boldsymbol{\theta}}_2 \tag{2.21}$$

while the force function ω in polar coordinates centered in P_2, becomes:

$$\omega = \frac{1}{1+e\cos(f)}\left[\frac{1}{2}\left(r_2^2+2(1-\mu)r_2\cos(\theta_2)+(1-\mu)^2\right)+\frac{1-\mu}{r_1}+\frac{\mu}{r_2}+\frac{1}{2}\mu(1-\mu)\right] \tag{2.22}$$

with

$$r_1 = \sqrt{r_2^2+2r_2\cos(\theta_2)+1}$$

The position of the third particle can be written in vector form as follows:

$$\boldsymbol{\xi} = r_2\hat{\boldsymbol{r}}_2 + (1-\mu)\hat{\boldsymbol{i}}$$

recalling also eqs. (2.16) - (2.21) it is possible to obtain $\boldsymbol{\xi}'$ and $\boldsymbol{\xi}''$. By inserting all the computed quantities into eqs.(2.11) and (2.12), the polar form of the equation of motion with reference system centered in P_2 is obtained.

$$r_2'' - r_2\theta_2'^2 - 2r_2\theta_2' = (1-\mu)\cos(\theta_2)\left(1-\frac{1}{r_1^3}\right)+r_2\left(1-\frac{1-\mu}{r_1^3}\right)-\frac{\mu}{r_2^3} \tag{2.23}$$

$$r_2\theta_2'' + 2r'\theta' - 2r_2' = (1-\mu)\sin(\theta_2)\left(\frac{1}{r_1^3}-1\right) \tag{2.24}$$

By solving these equation, the angle θ_2 is obtained. Using such information, the integration can be interrupted at a generic anomaly f^* if:

$$|\theta_2(f^*) - \theta_2(f_0)| = 2\pi$$

This means in fact that, at the current anomaly $f^* \leq f_{\text{lim}}$ (or $f^* \geq f_{\text{lim}}$ for negative stable sets) a complete revolution around P_2 has been accomplished. In this way, the integration of the equations until f_{lim} is avoided [4] and only the condition on the Kepler energy $H_2(f^*)$ mus be still verified. Recalling that the absolute angular velocity with respect to the sidereal reference frame is given by the summation $\theta_2' + \alpha'$ (with $\alpha' = 1$), the square velocity can be written in polar coordinate as:

$$v(f^*)^2 = r_2'(f^*)^2 + r_2(f^*)^2\left[\theta_2'(f^*)^2+1\right]^2$$

then the Kepler energy can be evaluated using eq. (2.1). By using this approach, a stable condition is immediately detected and the successive initial conditions

[4] Except when $f^* = f_{\text{lim}}$, however if this case occurs, f_{lim} has been probably chosen too small (or too high, if negative stable sets are considered).

can be analyzed. If simultaneously this procedure is applied to identify also the revolutions of the third particle around P_1, the primary interchange escapes can be found. Therefore, if the same approach is used, this kind f events can be detected without carrying on the integration of the equations until f_{lim} is reached. In this way it is avoided also the possibility that the spacecraft escapes from P_2, makes a complete revolution around P_1, then comes back to P_2 and makes a revolution around this primary with a negative value of H_2. For the definition of ballistic capture, the initial conditions producing this sort of trajectories are considered unstable, but if only the revolutions around $P-2$ are checked, the computational algorithm would consider them as stable. For this reason, the necessity of having also a continuous function $\theta_1(f)$ is now clear. The solution adopted to obtain this angle is the same used for $\theta_2(f)$; then also the equations in polar coordinates centered at P_1 are necessary

2.5.1 Equations of motion in polar coordinates centered in P_1

The same procedure used for P_2 can be applied to fine the polar equations of motion centered in P_1. This new reference system can be seen in Figure 1.4. In this case the relations between the old unit vectors and the new ones are:

$$\hat{\boldsymbol{r}}_1 = \cos(\theta_1)\hat{\boldsymbol{i}} + \sin(\theta_1)\hat{\boldsymbol{j}} \tag{2.25}$$
$$\hat{\boldsymbol{\theta}}_1 = -\sin(\theta_1)\hat{\boldsymbol{i}} + \cos(\theta_1)\hat{\boldsymbol{j}} \tag{2.26}$$

then, similarly to what done before, the derivatives with respect to the true anomaly are computed:

$$\hat{\mathbf{r}}_1' = \theta_1'\hat{\boldsymbol{\theta}}_1 \tag{2.27}$$
$$\hat{\boldsymbol{\theta}}_2' = -\theta_1'\hat{\boldsymbol{r}}_1' \tag{2.28}$$

and

$$\hat{\boldsymbol{r}}_1'' = -\theta_1'^2\hat{\boldsymbol{r}}_1' + \theta_1''\hat{\boldsymbol{\theta}}_1 \tag{2.29}$$
$$\hat{\boldsymbol{\theta}}_1'' = -\theta_1''\hat{\boldsymbol{r}}_1 - \hat{\boldsymbol{r}}_1'^2\hat{\boldsymbol{\theta}}_1 \tag{2.30}$$

The relation between the position in the synodic reference frame and in the polar one is the following:

$$\boldsymbol{\xi} = r_1\hat{\boldsymbol{r}}_1 - \mu\hat{\boldsymbol{i}} \qquad \longrightarrow \qquad \begin{cases} \xi = r1\cos(\theta_1) - \mu \\ \eta = r_1\sin(\theta_1) \end{cases} \tag{2.31}$$

Using these last equations, the force function ω in polar coordinate centered in P_1 assumes the form:

$$\omega = \frac{1}{1+e\cos(f)}\left[\frac{1}{2}\left(r_1^2 - 2\mu r_1\cos(\theta_1) + \mu^2\right) + \frac{1-\mu}{r_1} + \frac{\mu}{r_2} + \frac{1}{2}\mu(1-\mu)\right] \quad (2.32)$$

The definition of the gradient in polar coordinates can be obtained from the one given for P_2, just changing (r_2, θ_2) with (r_1, θ_1). The derivatives of the vector expression on the left-hand side of eq. (2.31) can be derived with respect to the true anomaly and substituted in the equations of motion for the synodic reference frame (see eqs. (2.11) and (2.12)) written in vector form. Therefore the polar equations of motion centered in P_1 are obtained:

$$r_1'' - r_1\theta_1'^2 - 2r_1\theta_1' = \mu\cos(\theta_2)\left(\frac{1}{r_2^3} - 1\right) + r_1\left(1 - \frac{1-\mu}{r_1^3}\right) - \frac{1-\mu}{r_1^3} \quad (2.33)$$

$$r_1\theta_1' + 2r_1'\theta_1' - 2r_1' = \mu\sin(\theta_2)\left(1 - \frac{1}{r_2^3}\right) \quad (2.34)$$

with

$$r_2 = \sqrt{r_1^2 - 2r_1\cos(\theta_1) + 1}$$

If these equations are integrated together with the system formed by eqs. (2.23) and (2.24) it is possible to detect not only when ballistic capture occurs, but also, by analyzing the angle θ_1, when a primary interchange escape (PIE) happens:

$$\left|\theta_2(\tilde{f}) - \theta_1(f_0)\right| = 2\pi$$

When this last relation is verified, being in fact $\tilde{f} \leq f_0$ (or $\tilde{f} \geq f_0$ when n-stable sets with $n \leq 1$ are studied), it is normally possible to break the integration process before f_{lim} is reached: by definition, if a PIE occurs, a ballistic capture can no longer occur.

The integration of both system of equations causes a longer integration time but it features the advantage that in this way a value of f_{lim} high enough can be set: for the most part of the initial conditions, either a ballistic capture or a PIE will usually occur. Using this approach, the computation time is extremely lower than that necessary if the equations of motion in cartesian coordinates would be integrated until f_{lim} is reached: the most part of the stable conditions are in fact already found during the first instants of integration [22].

2.5.2 Initial conditions in polar coordinates

While the polar equations of motion have been written both centered in P_1 and P_2, the relative initial conditions have still to be found. In the synodic reference frame, IC are given by eqs. (2.7) and (2.8), here after recalled:

$$\begin{cases} \xi = 1 - \mu + r_2 \cos(\theta_2) \\ \eta = r_2 \sin(\theta_2) \end{cases} \qquad \begin{cases} \xi' = -v \sin(\theta_2) + r_2 \sin(\theta_2) \\ \eta' = v \cos(\theta_2) - r_2 \cos(\theta_2) \end{cases}$$

where the velocity v is obtained from (2.6):

$$v = \sqrt{\mu \frac{1+e}{r_2}}$$

Recalling what said in section 2.2, for a fixed initial vale of true anomaly f_0, the initial conditions are completely given once the angle θ_2, the distance from the secondary primary r_2 and the eccentricity of the initial elliptic orbit e have been chosen. Therefore, the value of $r_2(f_0)$ and of $\theta_2(f_0)$ are obtained through the definition of stable set. The same definition states also that, being the starting position of the spacecraft at the pericenter of the initial elliptic orbit, the initial velocity is *normal* to the semi-major axis of the ellipse (see Figure 2.2), then the velocity along the direction $\hat{\boldsymbol{r}}_2$, which in the initial instant is coincident with the periapsis of the ellipse, is zero, consequently $r_2'(f_0)$ is null as well. Therefore it can be calculated by simply dividing v by r_2 and, recalling that v is referred to the *sidereal* reference frame centered in P_2, the angular velocity due to the rotation of the synodic reference frame, $\alpha' = 1$, must be subtracted. Doing so, the initial conditions for the polar system centered in P_2 are all explicated. They are reported hereafter for a clear understanding:

$$\begin{cases} r_2(f_0) = r_i \\ \theta_2(f_0) = \theta_j \end{cases} \qquad \begin{cases} r_2'(f_0) = 0 \\ \theta_2'(f_0) = \sqrt{\mu \frac{1+e_k}{r_i^3}} - 1 \end{cases} \tag{2.35}$$

Once the initial conditions for the system centered in P_2 are evaluated, it is possible to calculate the corresponding initial conditions for the polar system centered on the other primary. In order to understand the equations that are going to be reported, Figure 2.4 might be helpful.

Thanks to geometrical considerations it is possible to write the following general relations between the two different systems of polar coordinates:

$$\begin{aligned} r_1 &= \sqrt{r_2^2 + 2 r_2 \cos(\theta_2) + 1} \\ \theta_1 &= \tan^{-1}\left(\frac{r_2 \sin(\theta_2)}{r_2 \cos(\theta_2) + 1} \right) \end{aligned}$$

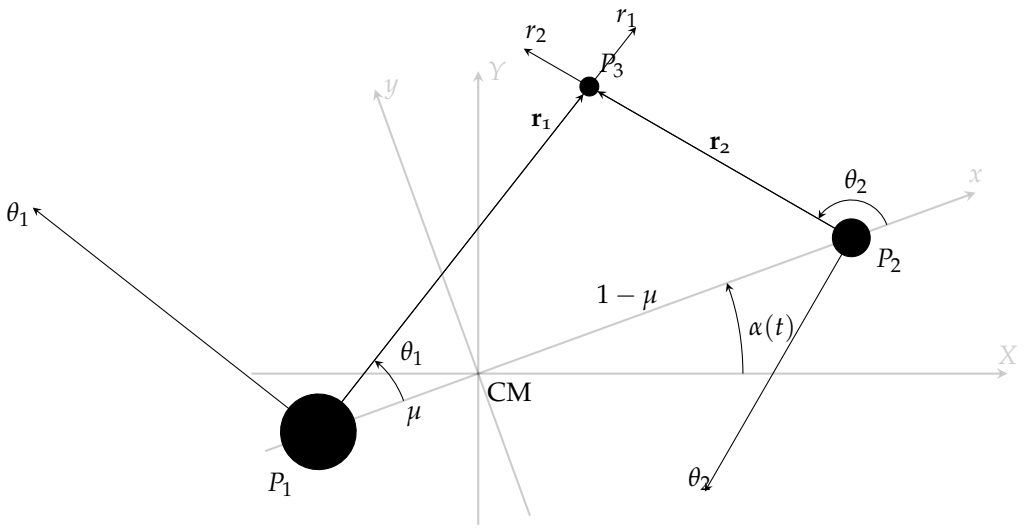

Figura 2.4: Summary of the two kind of polar reference frame analyzed so far, the former centered in P_1, the latter in P_2

In the same way, for the velocity the following expressions are obtained:

$$\begin{aligned} r_1' &= r_2' \cos(\theta_2 - \theta_1) - r_2\theta_2' \sin(\theta_2 - \theta_1) \\ \theta_1' &= \frac{r_2\theta_2'}{r_1} \cos(\theta_2 - \theta_1) + \frac{r_2'}{r_1}\theta_2' \sin(\theta_2 - \theta_1) \end{aligned}$$

Recalling thatn eq. (2.35), which is valid only when $f = f_0$, the initial conditions for the polar reference system centered in P_1 become:

$$r_1(f_0) = \sqrt{r_i^2 + 2r_i \cos(\theta_j) + 1} \tag{2.36}$$

$$\theta_1(f_0) = \tan^{-1}\left(\frac{r_i \sin(\theta_j)}{r_i \cos(\theta_j) + 1}\right) \tag{2.37}$$

and

$$r_1'(f_0) = r_i\theta_2'(f_0) \sin(\theta_j - \theta_1) \tag{2.38}$$

$$\theta_1'(f_0) = \frac{r_i\theta_2'(f_0)}{r_1(f_0)} \cos(\theta_j - \theta_1(f_0)) \tag{2.39}$$

In this section, the equations for the problem in polar coordinates have been illustrated together with the corresponding initial conditions. As mentioned before, there is the possibility that a regularization is necessary. The detailed treatment of the, as already said, *local* regularization according to Levi-Civita approach is reported in The previous chapter in section 2.2.

2.6 COMPUTATION OF WEAK STABILITY BOUNDARIES

The equations involved in calculations of stable sets and weak stability boundaries have been all written In order to give a clear vision of all the equations used with the corresponding reference systems, they are all summarized hereafter, starting from those written in polar coordinates centered in P_2:

$$\begin{aligned} r_2'' - r_2\theta_2'^2 - 2r_2\theta_2' &= (1-\mu)\cos(\theta_2)\left(1-\frac{1}{r_1^3}\right) + r_2\left(1-\frac{1-\mu}{r_1^3}\right) - \frac{\mu}{r_2^3} \\ r_2\theta_2'' + 2r'\theta' - 2r_2' &= (1-\mu)\sin(\theta_2)\left(\frac{1}{r_1^3}-1\right) \end{aligned}$$

with

$$r_1 = \sqrt{r_2^2 + 2r_2\cos(\theta_2) + 1}$$

and initial conditions given by:

$$\begin{cases} r_2(f_0) = r_i \\ \theta_2(f_0) = \theta_j \end{cases} \qquad \begin{cases} r_2'(f_0) = 0 \\ \theta_2'(f_0) = \sqrt{\mu\dfrac{1+e_k}{r_i^3}} - 1 \end{cases}$$

At th same time the equations in polar coordinates centered in P_1 are solved:

$$\begin{aligned} r_1'' - r_1\theta_1'^2 - 2r_1\theta_1' &= \mu\cos(\theta_2)\left(\frac{1}{r_2^3}-1\right) + r_1\left(1-\frac{1-\mu}{r_1^3}\right) - \frac{1-\mu}{r_1^3} \\ r_1\theta_1' + 2r_1'\theta_1' - 2r_1' &= \mu\sin(\theta_2)\left(1-\frac{1}{r_2^3}\right) \end{aligned}$$

with

$$r_2 = \sqrt{r_1^2 - 2r_1\cos(\theta_1) + 1}$$

and initial conditions corresponding to those of the polar system centered at P_2, properly transformed in this new reference systems

$$\begin{cases} r_1(f_0) = \sqrt{r_i^2 + 2r_i\cos(\theta_j) + 1} \\ \theta_1(f_0) = \tan^{-1}\left(\dfrac{r_i\sin(\theta_j)}{r_i\cos(\theta_j)+1}\right) \end{cases} \qquad \begin{cases} r_1'(f_0) = r_i\theta_2'(f_0)\sin(\theta_j - \theta_1) \\ \theta_1'(f_0) = \dfrac{r_i\theta_2'(f_0)}{r_1(f_0)}\cos(\theta_j - \theta_1(f_0)) \end{cases}$$

The equations just written are integrated simultaneously until either the spacecraft completes a revolution around P_1 or P_2 or when the limit true anomaly f_{lim} is reached. Furthermore, these equations are no longer considered when the third particle flies near one of the primary, since in this case the equations of the regularized systems are exploited. There is one more topic to be investigated: the boundary which separates the regularized from the non-regularized regions. Such boundary is identified by the so called *Levi-Civita circle*. When the spacecraft is traveling inside this region, that is when $r_i \leq r_{LC,i}$, the regularized equations of motion must be taken into account.

It must be said that, during the integration of the regularized system, the occurrence of a PIE or a ballistic capture cannot be instantaneously verified. The equations in the u, v-plane are in fact derived from the synodic, cartesian reference system (ξ, η), so, in obtaining a continuous function for $\theta_1(f)$ and $\theta_2(f)$, they features the same problem discussed in section 2.4. For this reason, the above mentioned events can be detected only when the spacecraft leaves the Levi-Civita circles, that is when $r_i > r_{LC,i}$, and the regularized variables are converted into the polar ones [5], where the presence of such events can be verified. Another consequence is that, if the spacecraft remains always inside the Levi-Civita circle, the regularized equations must be integrated until f_{lim} is reached. This is a drawback, however for small value of the mass parameter μ, it happensa only when the initial conditions with the smallest values of r_i are considered. Moreover, the integration of the regularized equations of motion, despite the large f span, proceeds faster than the equations in polar coordinates, as verified during the calculations of stable sets. This happens also because the presence of trigonometric functions inside the polar equations makes the integration a little bit slower (*Topputo* e *Belbruno* [16]).

[5] There is an intermediate step within this transformation, that is the conversion to the cartesian coordinates.

3 MANIPULATION OF BALLISTIC CAPTURE: THE ROBUSTNESS ANALYSIS

In this chapter the concept of capture set is recalled. After the illustration of the properties related to orbits with prescribed behavior, which must accomplish a precise number of passages around the secondary primary, the procedure applied to assess the robustness of the method is presented. This aspect of the problem is of utmost importance. In fact, if a ballistic capture orbit results to be invariant with respect to a perturbation of the initial conditions, it becomes a very good candidate for an interplanetary mission designed with this purpose. As already said, the perturbation of the initial conditions, which will be performed with a statistical approach, is the tool to assess the adequateness of an orbit and, by extension, of the entire set. This aspect must be considered in addiction to the strict dependence of this kind of orbits on the eccentricity and the initial true anomaly. It will be shown that these actors strongly influence the size and the shape of the sets and, furthermore, the behavior of orbits propagated from the perturbed initial conditions.

3.1 THE CAPTURE SETS

As one can easily sense, a capture orbit consists in a curve reaching the selected primary from the deep space and performing a certain number of revolutions about it. This happens only by means of purely gravitational interactions between the spacecraft and the primaries. The number of passages is strictly related to the mission purpose. Therefore a space probe designed for planetary observation requires several of them.

However, it is necessary to define the capture set from a mathematical point of view. To achieve this task, some concepts still need to be introduced. In the previous chapter the stable and unstable sets have been treated and, for sake of clarity, the key topics will be briefly recalled. A set is said to be stable if a certain number of orbits are performed about the considered primary and the Keplerian energy H_2 undergoes a reduction for two consecutive passage across the line $l(\theta_2)$, while it is considered unstable if an orbit about the *first* primary is performed and the energy keeps on increasing (see Figure 2.3). Starting from certain initial conditions, a capture set results from the intersection of a backward unstable set and a forward stable one. By labeling the unstable set as $\mathcal{X}(e, f_0)$ it results:

$$\mathcal{C}^n_{-1}(e, f_0) = \mathcal{X}_{-1}(e, f_0) \cap \mathcal{W}_n(e, f_0) \tag{3.1}$$

The initial conditions in $\mathcal{C}^n_{-1}(e, f_0)$ generate orbits that, in order:

1. Escape the target when integrated backward, or equivalently approach the target in forward integration coming from the deep space;
2. Perform n revolutions about the target primary without escaping or impacting it.

This is desirable in preliminary mission analysis, as orbits with this behavior may be good candidates to design a ballistic capture upon arrival. It must be noted that the definition of capture set reported in eq. (3.1) exhibits a dependence on the *osculating orbit eccentricity* and *initial true anomaly* of the primaries system. In fact these actors play a role of utmost importance. In particular:

- Depending on the osculating orbit eccentricity, the capture sets computed in the elliptic model are generally larger than those computed in the circular model. Moreover, the occurrence of capture orbits in the total set of initial condition strongly increase for increasing e. Unfortunately, the great drawback caused by considering a non-circular model lies in the fact that the time span within which the revolutions are completed is much shorter with respect to the circular model.
- On the other hand, the role played by the true anomaly consists in an increasing size of the capture set as the value of f_0 gets bigger for prograde orbits. The results that will be presented will confirm such statements.

3.2 PROBLEM DEVELOPMENT

The selected primaries for the robustness analysis of ballistic capture orbits are the *Sun and Mars*. According to this choice, the mass parameter μ and the eccentricity of the orbits of such primaries are immediately defined. However, for sake of completeness, an overview of the characteristic parameters of the possible primaries which can be selected to perform an analogous analysis are reported in Table 1.

In order to perform the robustness analysis, a proper capture set must be used. By applying the entire procedure illustrated in the previous chapter, the Weak Stability Boundaries have been obtained. By backward integration, it has been analyzed which initial conditions produce an escape trajectory, that is which initial conditions belongs to the unstable set $\mathcal{W}_{-1}(e, f_0)$. Accordingly, the capture sets have been defined. As said before, the Weak Stability Boundary is strictly dependent on the eccentricity of the osculating orbit and on the initial true anomaly, that is the relative position of the two primaries. The combinations used in this work are reported in Table 2. Note that f_0 is expressed as multiple of π. The choice for this range of e and f_0 lies in the fact that a high-valued eccentricity orbit is much more prone to be selected as an interplanetary transfer orbit. In fact, the higher e is, the more the capture path become similar to a hyperbola, which is the well known orbit typology experienced by a spacecraft as it cross the target planet sphere of influence. On the other hand, the limitation of the analysis to the first quadrant is enough to point out the most

Tabella 1: Physical parameters of Solar System planets. Mars and its characteristic quantities are highlighted in gray.

Planet	Radius [km]	Gravitational parameter [km³/s²]	Eccentricity	Mass Parameter
Mercury	2439.7	$2.203 \cdot 10^4$	0.2056	$1.660 \cdot 10^{-7}$
Venus	6051.8	$3.249 \cdot 10^5$	0.0068	$2.448 \cdot 10^{-6}$
Earth	6371	$3.986 \cdot 10^5$	0.0167	$3.003 \cdot 10^{-6}$
Mars	3389.5	$4.283 \cdot 10^4$	0.0934	$3.2274 \cdot 10^{-7}$
Jupiter	69911	$1.267 \cdot 10^8$	0.0484	$9.537 \cdot 10^{-4}$
Saturn	58232	$3.794 \cdot 10^7$	0.0542	$2.857 \cdot 10^{-4}$
Uranus	25362	$5.795 \cdot 10^6$	0.0472	$4.366 \cdot 10^{-5}$
Neptune	24622	$6.837 \cdot 10^6$	0.0086	$5.151 \cdot 10^{-5}$

outstanding features of the capture orbits and to prove their feasibility by perturbing the initial conditions.

Tabella 2: Combination of eccentricity and initial true anomaly used to compute the capture sets

Set index	Eccentricity e	Initial true anomaly f_0
`f000pi_e90`	0.90	0
`f000pi_e99`	0.99	0
`f025pi_e90`	0.90	0.25π
`f025pi_e99`	0.99	0.25π
`f050pi_e90`	0.90	0.50π
`f050pi_e99`	0.99	0.50π
Required number of passages around Mars: 6		

The procedure adopted to compute the set with parameters in Table 2 is hereafter reported:

1. The *one time stable* set $\mathcal{W}_1(e, f_0)$ is computed;
2. Starting from the results obtained for the $\mathcal{W}_1(e, f_0)$, the forward propagation is performed. Only *six time stable* sets $\mathcal{W}_1^6(e, f_0)$ are retrieved.
3. To assess the ballistic capture it is necessary that backward propagation of motion produces an escape orbit. Accordingly, the acceptable initial conditions inside the Weak Stability Boundary reduce in number. By integrating and retrieving the *one time unstable set* it is possible to eventually construct the capture sets $\mathcal{C}_{-1}^6(e, f_0)$.

Having the purpose to exploit the ballistic capture for a future interplanetary mission, the robustness analysis must be performed *sufficiently far* from Mars. Therefore, the backward integration represents the starting point for the application of a perturbation on the state vector. It has been chosen to propagate the initial conditions inside the Weak Stability Boundary up to the Sphere of influence of Mars. The reason for this is that such distance, *within an unperturbed space environment*, represent a good compromise between accuracy of the results with respect to their initial formulation and sufficiently high distance such that no OCM [1] are necessary. In fact it has been noted that, by integrating forward the initial conditions at the Sphere of Influence, results are shifted by about $10^{-7}\,\% - 10^{-8}\,\%$[2] with respect to the forward integration of the initial conditions belonging to the Weak Stability Boundary. Despite this discrepancy, the behavior of the orbits propagated from the IC at the Sphere of Influence is the same as the *nominal ones*. Moreover, neither crashes over the surface of Mars, neither ballistic escape have been found at this stage.

As mentioned before, the dimension of the capture sets are much bigger for high values of eccentricity of the osculating orbit and initial true anomaly. In order to make this aspect more evident and clearer, the number of initial conditions producing a ballistic capture as function of e and f_0 have been reported in the histogram in Figure 3.1. It is evident that the thickest condition is found for $e = 0.99$ and $f_0 = 0.5\pi$. However, the greatest drawback is represented, as it will be shown later, by the increased instability in the behavior of the orbits. As a confirmation of this fact, the capture sets obtained through the procedure illustrated above is reported in Figure 3.2.

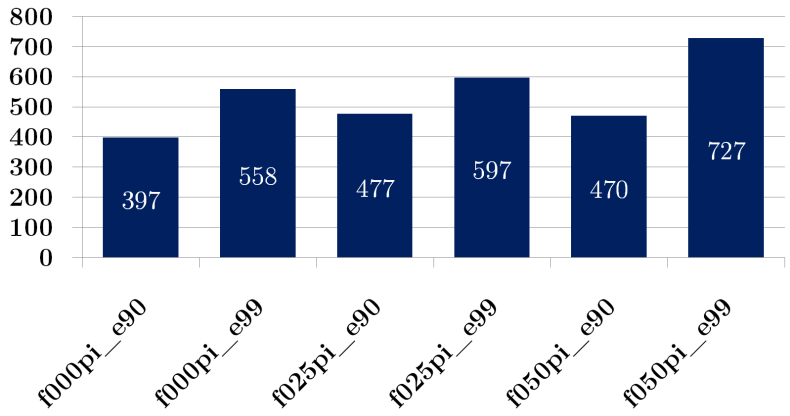

Figura 3.1: Summary plot of the number of initial conditions according to the value of eccentricity and initial true anomaly.

[1] Orbital Correction Maneuvers.

[2] Such percentage are just apparently low. In fact the gap between the nominal and the perturbed conditions spans from $\mathcal{O}(10^0)\,m$ to $\mathcal{O}(10^3)\,m$

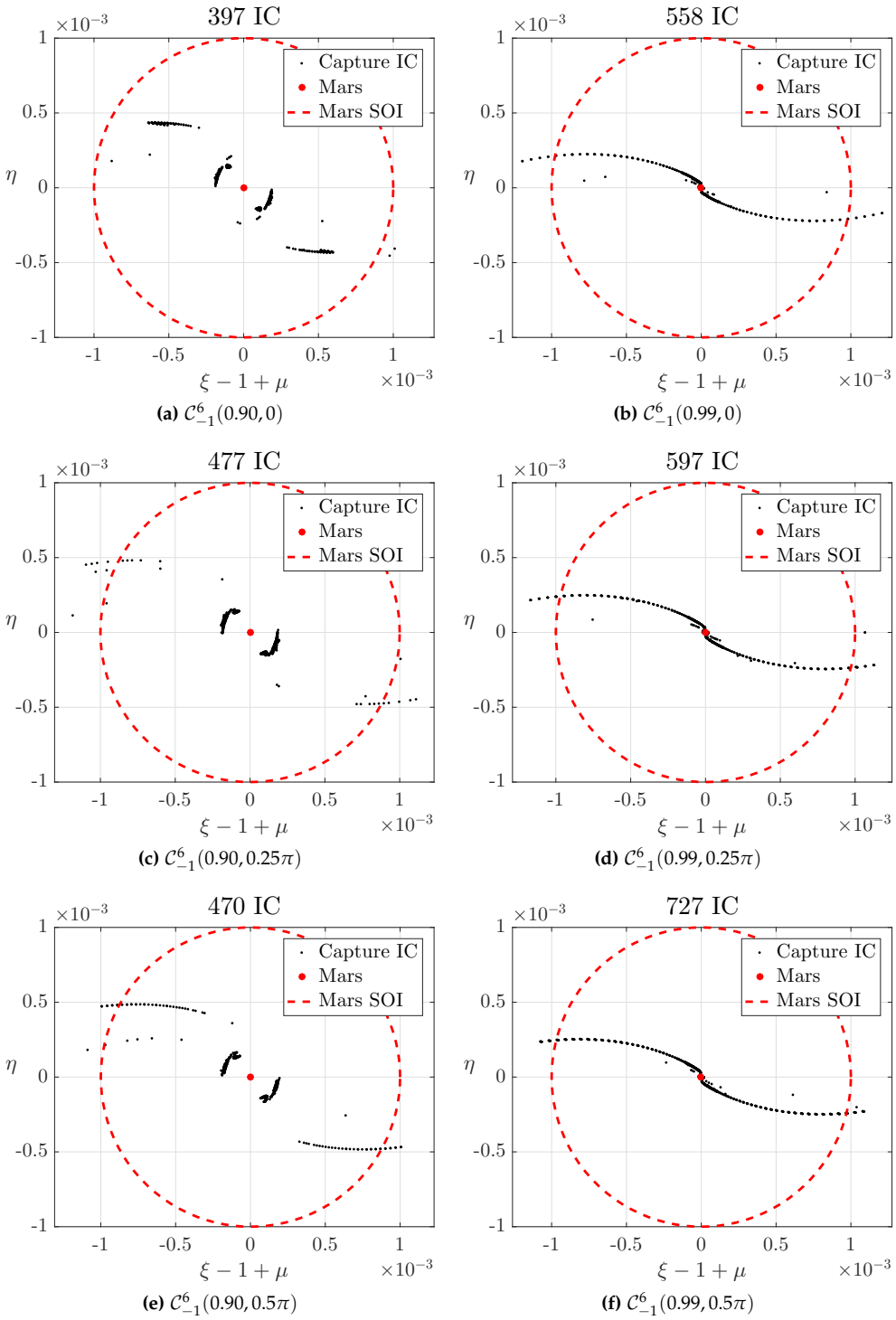

(a) $\mathcal{C}^6_{-1}(0.90, 0)$ **(b)** $\mathcal{C}^6_{-1}(0.99, 0)$

(c) $\mathcal{C}^6_{-1}(0.90, 0.25\pi)$ **(d)** $\mathcal{C}^6_{-1}(0.99, 0.25\pi)$

(e) $\mathcal{C}^6_{-1}(0.90, 0.5\pi)$ **(f)** $\mathcal{C}^6_{-1}(0.99, 0.5\pi)$

Figura 3.2: Representation of the capture sets capture sets computed by exploiting the parameters reported in Tab. 1. As it can be easily noted, the size of the set strongly increase for increasing eccentricity of the osculating orbit and true anomaly. Note that the dimensions of Mars are not the real one. It has been deliberately not properly scaled in order to keep it visible

Orbits resulting from the *up-to-the-SOI-propagated* initial conditions are essentially of two kind.

- *Regular ballistic capture orbits*, featuring a quite regular behavior for the considered time/true anomaly span. There are no sudden change in directions due to gravitational interaction and the curve preserves a quite smooth and regular profile. By looking at the nominal configuration, it can be noted that, for the *low* value of the eccentricity of the osculating orbit, that is $e = 0.90$, the variation of initial true anomaly does not produce a significant effect over the orbital path. On the other hand, osculating orbits featuring a *high* eccentricity, $e = 0.99$, are characterized by a less regular trend and, in general, they much bigger than those shown before. Also in this case, different values of true anomaly do not alter significantly the curve shape. It will be shown that this kind of orbits are very robust with respect to the perturbation of the initial conditions. Some examples are represented in Figure 3.2 (covering the current and the next page).

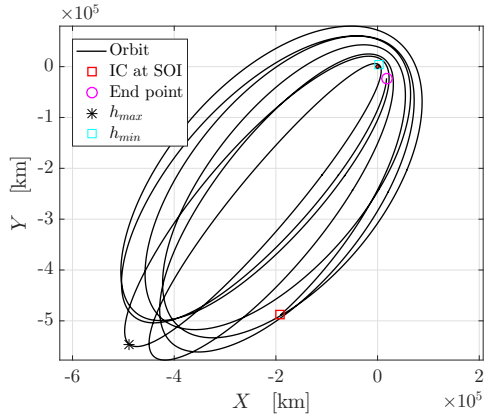

(a) $f_0 = 0$; $e = 0.90$

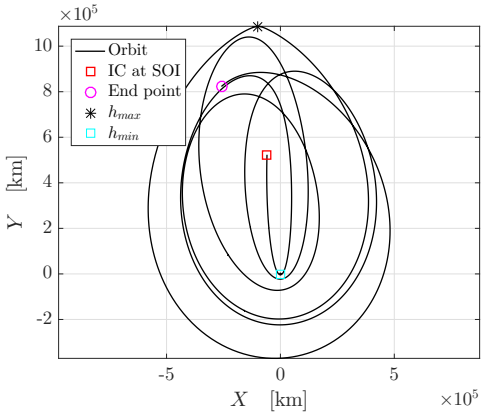

(b) $f_0 = 0$; $e = 0.99$

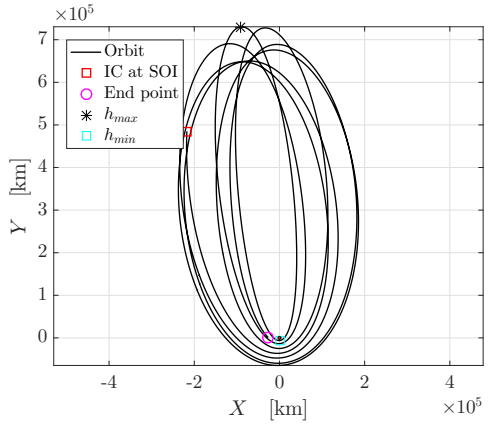

(c) $f_0 = 0.25\pi$; $e = 0.90$

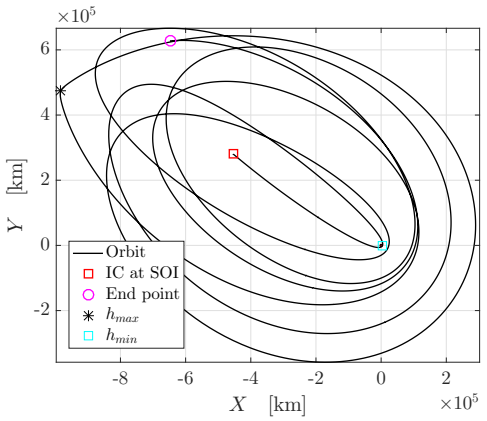

(d) $f_0 = 0.25\pi$; $e = 0.99$

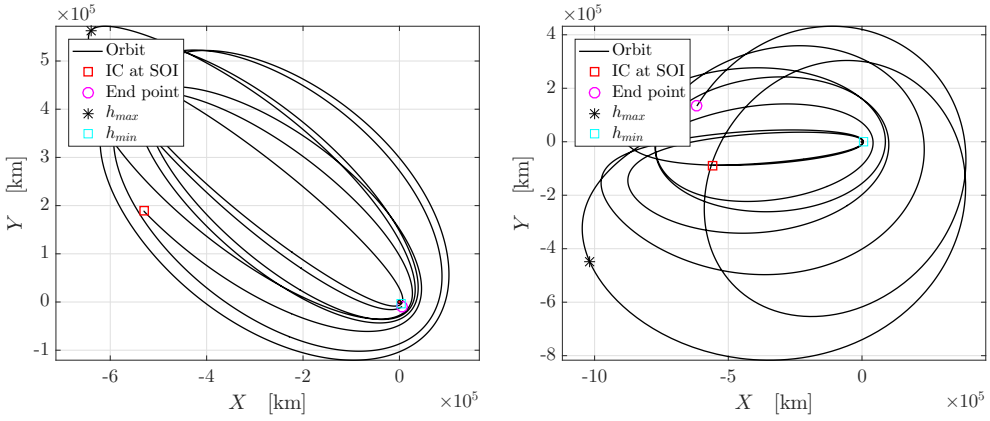

(e) $f_0 = 0.50\pi$; $e = 0.90$ **(f)** $f_0 = 0.50\pi$; $e = 0.99$

Figura 3.2: Examples of regular ballistic capture orbits retrieved from the initial conditions for each computed capture set. For each one, the starting and the end point of the integration, the highest and the lowest altitude locations have been highlighted.

- *Acrobatic ballistic capture orbits*, following a definitely non-regular path about the primary. Differently from the regular ballistic capture orbits, both the augmentation of the osculating orbit eccentricity and the variation of the initial true anomaly lead to very significant change in the orbital path shape. In particular, sudden change in directions and loop in the shape of the curve are very frequent. Moreover, these kind of orbits are much less stable with respect to a perturbation of the initial state vector, thus producing several crashes and ballistic ejections. As for the regular orbit, an exemplification is represented in Figure 3.2.

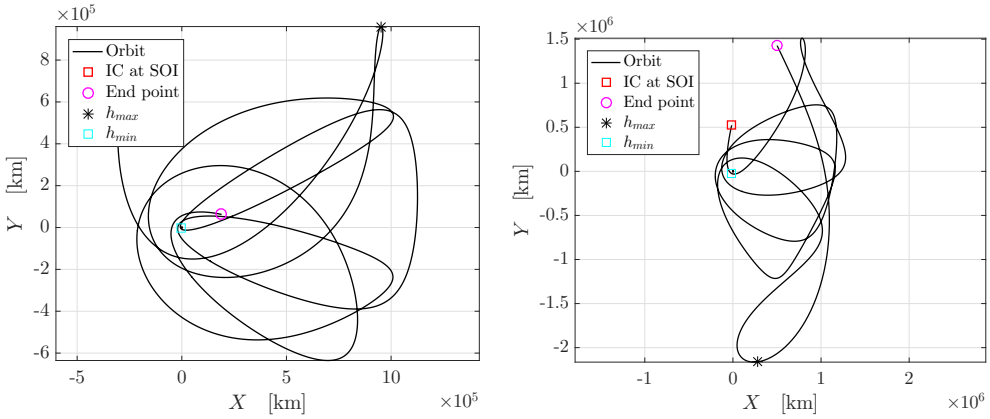

(a) $f_0 = 0$; $e = 0.90$ **(b)** $f_0 = 0$; $e = 0.99$

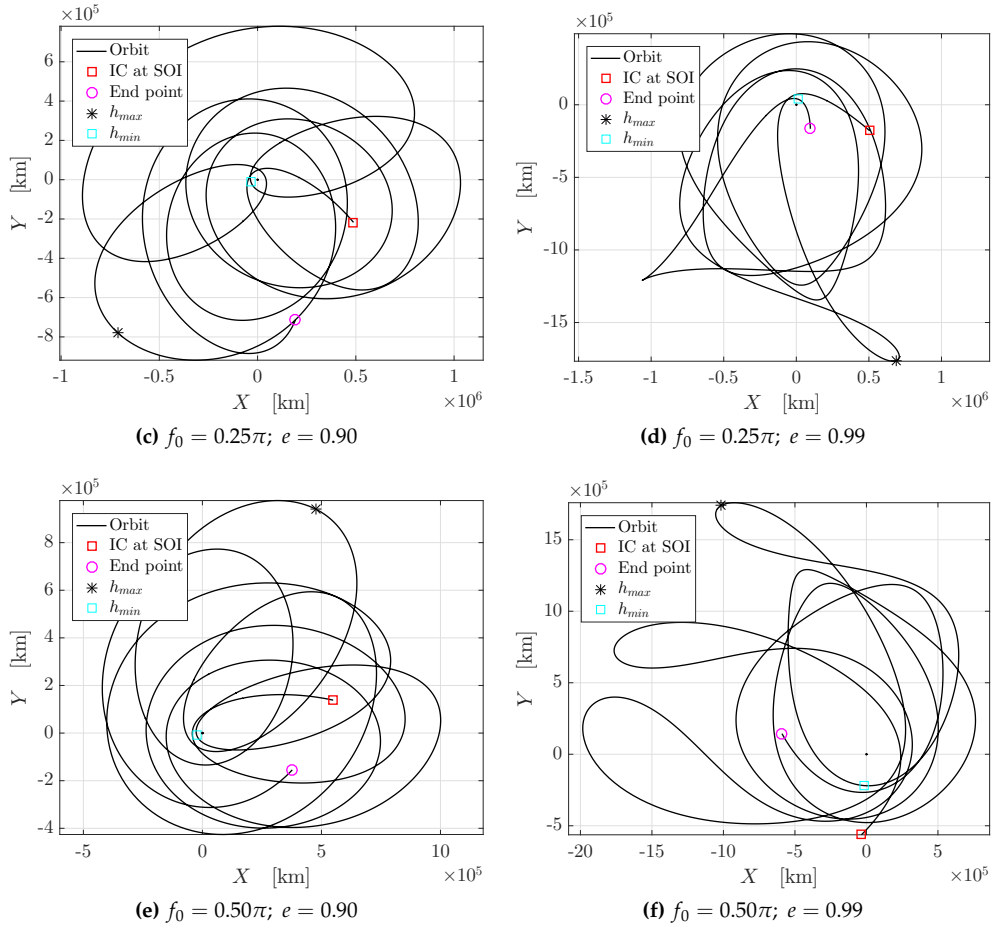

(c) $f_0 = 0.25\pi;\ e = 0.90$ **(d)** $f_0 = 0.25\pi;\ e = 0.99$

(e) $f_0 = 0.50\pi;\ e = 0.90$ **(f)** $f_0 = 0.50\pi;\ e = 0.99$

Figura 3.2: Examples of acrobatic ballistic capture orbits retrieved from the initial conditions for each computed capture set. For each one, the starting and the end point of the integration, the highest and the lowest altitude locations have been highlighted.

As final remark it must be pointed out that these last results have been represented within a *sidereal*, that is inertial, *reference frame* centered in Mars. The reason for this lies in the fact that this representation allows a much clearer view of the orbit and its behavior as the independent variable f increase during the integration procedure. Moreover, the target primary is located at the origin of the axes, thus leading to an easier interpretation of the results since the primary is not moving and the spacecraft does not *follow* it. For sake of clarity, computations have not been achieved in this coordinate systems, but polar coordinates have been exploited (see Chapter 2 for a detailed treatment.)

3.3 PERTURBATION OF THE INITIAL STATE AND ANALYSIS OF THE RESULTS

So far, the basis of the robustness analysis with all the related considerations has been presented. The core of the problem is being treated in this section. As mentioned before, this part of the work aims to analyze the effect that a perturbation of the initial conditions produces over the ballistic capture orbits. To achieve the perturbed state vector, a statistical approach has been adopted. The requirement of the perturbations, and consequently the principal aspect of the robustness analysis, is that a *non-deterministic* variation must be considered. As it will be shown later, the results of this step consist in the generation of a population of initial conditions featuring a certain mean value and a fixed variance.

Before presenting the procedure adopted to obtain such populations, a brief survey about the dispersion of a set of data values will be hereafter recalled. Considering a large number of independent measurements, their distribution tends towards the so called *normal distribution* or *Gaussian distribution*. The governing equation of this particular distribution is the Gaussian function

$$f(x, \mu, \sigma) = \frac{1}{\sigma\sqrt{2\pi}} \exp\left[-\frac{(x-\mu)^2}{2\sigma^2}\right] \tag{3.2}$$

where x is the independent variable, μ is the mean value of the distribution and σ is the variance of such distribution. Among the advantages lying in the usage of normal distributed data is that there is no need to compute the *median* and the *mode*, since they are equal to the mean. As an example, a purely qualitative representation of a Gaussian curve is reported in Figure 3.3. As it can be noted, different values of variance have been considered. As σ decreases, the curve progressively shrinks and consequently the probability to find a member of the data set in correspondence of the mean value increases.

Since the samples of the data set are totally random quantity, then it is necessary to have an estimation of the number of samples effectively contained inside a selected interval inside the Gaussian curve. This can be overcome by introducing the concept of *confidence interval*. The procedure to compute such parameter is reported hereafter.

1. Compute the mean value and the variance, respectively:

$$\mu = \frac{\sum_1^N x}{N} \tag{3.3}$$

$$\sigma = \sqrt{\frac{\sum_1^N (x-\mu)^2}{N}} \tag{3.4}$$

2. The confidence level (CL) must be chosen. Typical values of confidence level are reported in Table 3

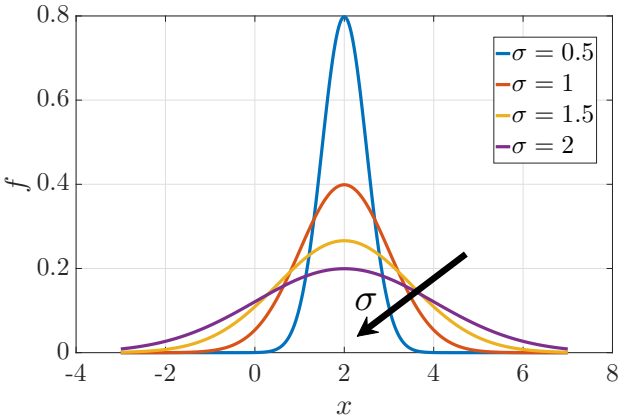

Figura 3.3: Gaussian curve of four kind of data set. The standard deviation variation is reported in the legend. For all the populations, the mean value is $\mu = 2$.

Tabella 3: #σ of the mean for a normal distribution. The shaded row indicates the confidence level used in this work.

#σ	**Confidence Interval**
1σ	84.13%
1.5σ	93.32%
2σ	97.73%
2.5σ	99.38%
3σ	99.87%
3.5σ	99.98%
$> 4\sigma$	100%

3. The margin of error (MoE) can be computed. Such parameter can be obtained from the knowledge of the size of the data set, the standard deviation and the selected confidence level:

$$MoE = CL\frac{\sigma}{\sqrt{N}} \tag{3.5}$$

4. The confidence interval results from the summation/subtraction from the mean value the computed margin of error, therefore:

$$CI = \mu \pm MoE \tag{3.6}$$

As mentioned before, the confidence level used in this work is 3σ of the mean.

After this brief theoretical review, the procedure adopted in this work can be analyzed. A spacecraft traveling through deep space features a certain state vector

which is affected of a certain degree of uncertainty because of it is composed of *measured* quantities. Such measurements are related to position and velocity, but typically only a fraction of total set of position and velocity components are actually retrieved. Moreover, they are corrupted by random and systematic errors. The device used for the position and velocity determination consist in on-board cameras or in telecommunication links between the spacecraft and Earth. Therefore the state vector is determined through *optical* and *radio-metric* measurements.

Typical examples of measurement techniques consist in (for a detailed analysis see *Turyšev* [17], the url is reported in the footnote[3]):

- Range and Doppler Tracking;
- Angular Tracking
- Interferometry;

For most interplanetary missions, the spacecraft position uncertainties is much smaller in the radial direction rather than in any angular one. Radial components of position and velocity are directly measured by range and Doppler observations. In absence of other data, angular components are much more difficult to determine. In fact they require either changes in geometry between the observer and and the spacecraft or additional simultaneous observer, neither of which is simple to accomplish. The immediate consequence for this is that angular errors are up to 10^3 times greater than radial errors even under the most favorable conditions, mostly when depending on range and Doppler measurements. Assuming this kind of measurements, the uncertainties for the state vector exploited in this work are reported in Table 4.

Tabella 4: Uncertainties for the state vector (Source: *Jet Propulsion Laboratory*)

Uncertainty type	Position	Velocity
Radial	2 m	0.1 mm/s
Angular	3 km	0.1 m/s

The link point between measurements and statistic approach is represented by the generation of a population of initial conditions which are dispersed according to the selected values of uncertainties with an accuracy of 3σ of the mean as mentioned before.

Since the uncertainties are known, the procedure adopted to generate the data set follows an inverse approach: the population is generated with a mean value correspondent to the nominal initial condition and a variance obtained from the uncertainties reported in 4 and the selected confidence interval. For the sake of coherence, even tough the initial conditions are written in polar coordinate in order to match with the uncertainty values, results will be plotted in cartesian coordinates.

[3] http://lnfm1.sai.msu.ru/~turyshev/lectures/lecture_9.0-Deep-Space-Navigation

In particular, as mentioned before, the sidereal reference frame is selected to illustrate the outcome of the analysis.

By labeling the uncertainties respectively as P_r for the radial one and P_α for the angular one, the variance in the correspondent direction is found:

$$\sigma_r = \left(\frac{P_r}{3}\right)^2 \qquad \sigma_\alpha = \left(\frac{P_\alpha}{3}\right)^2 \tag{3.7}$$

The variance value are reported in the following table:

Tabella 5: Results of eq. (3.7)

σ_r	σ_α
$4.45 \cdot 10^{-7}$	1

An example of produced dataset is reported in Figure 3.4

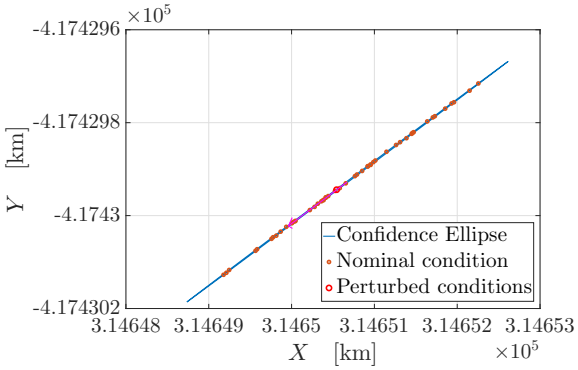

(a) Position

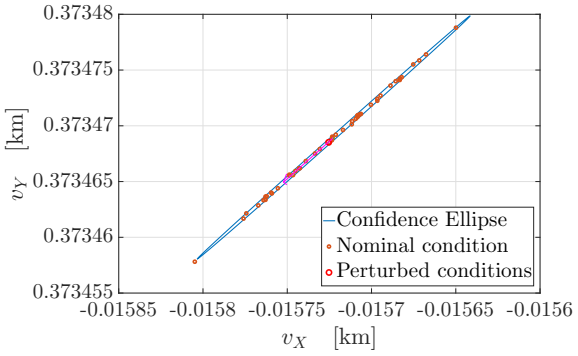

(b) Velocity

Figura 3.4: Dispersion map of the perturbed initial conditions. The reported initial conditions are retrieved from the capture set featuring $f_0 = 0$ and $e = 0.90$. As already mentioned, such data set is represented in the sidereal P_2-centered reference frame.

As it can be clearly seen, such ellipses features a minor axis much smaller than the major one. The reason must be searched in the fact that the radial uncertainties is much smaller than the angular one. Concerning these ellipse, there are some remarkable features to point out:

- The largest and the smallest eigenvalue of the variance matrix providing the direction of maximum and minimum variation. In the case presented in Figure 3.4:

Tabella 6: Maximum and minimum eigenvalues.

	λ_{max}	λ_{min}
Position	0.63877	$4.08206 \cdot 10^{-7}$
Velocity	$1.11487 \cdot 10^{-9}$	$1.02775 \cdot 10^{-14}$

- The orientation of the ellipse governed by the angle δ resulting from:

$$\delta = \tan^{-1}\left(\frac{\boldsymbol{v}_1(X)}{\boldsymbol{v}_1(Y)}\right) \tag{3.8}$$

where $\boldsymbol{v}_1$ is the eigenvector of the variance matrix that corresponds to the largest eigenvalue. Again, concerning the situation just presented the values of δ is:

Tabella 7: Uncertainties for the state vector (Source: *Jet Propulsion Laboratory*)

	Position	**Velocity**
$\boldsymbol{\delta}$	187.60^o	187.66^o

These values are justified by looking at the direction of the maximum eigenvector reported in the zoom of Figure 3.4

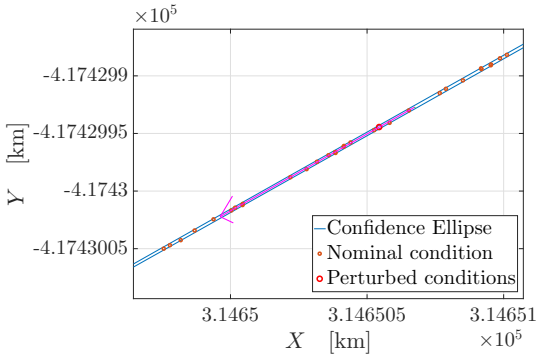

(a) $f_0 = 0;\ e = 0.90$

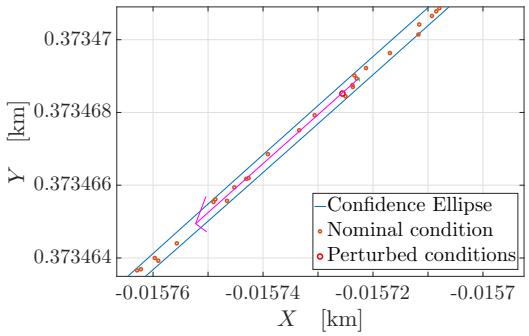

(b) $\mathcal{C}^6_{-1}(0.99, 0)$

Figura 3.4: Particular of the confidence ellipses in order to point out the direction of the maximum eigenvector to justify the values of δ.

As a family of initial conditions has been generated, it follows that a family of orbits is then produced. The most outstanding effect of the perturbation of the initial conditions is an alteration of the orbital path with respect to the nominal configuration. Three main effect have been found:

- The perturbed initial condition, when propagated forward, *still results in a ballistic capture orbit*, even if shifted with respect to te nominal one. The magnitude of the shifting strictly depends on the initial conditions.
- The perturbed trajectory *leads the spacecraft to crash* over the surface of Mars. Therefore the current initial condition cannot be a candidate for a ballistic capture and, consequently, is discarded. It has been noted that, as an average, crashes occur between the third and the fourth passage.
- A *ballistic ejection* orbit is produced from the altered initial conditions. In this case it is necessary to distinguish between orbits which escape once the prescribed passage about Mars have been accomplished and orbits ejecting the spacecraft from the Mars Sphere of Influence before the required number of rounds have been performed. Orbits belonging to the first category have been included within the candidate group of suitable orbits.

Hereafter some of the retrieved results will be presented and analyzed. First, the definition of robustness is provided. *A perturbed initial condition and, by extension, a ballistic capture orbit is robust with respect to the considered perturbation if neither crashes or escape occur for the entire true anomaly span considered.*

In order to analyze the behavior of the perturbed orbits, once again statistics has been exploited. In particular, it has been chosen to analyze the dispersion map of the state vector at a fixed station along the orbital path. Such station corresponds to the couple (r, θ_2) associated to the first closest passage over the surface of Mars. In other words, as the spacecraft approaches the first *relative* minimum along the orbit, the

associated state vector is retrieved and converted in polar coordinates. Consequently, the angle $\theta_2(\bar{f})$ (see Figure 2.2 for the details) is used as a reference for the successive passage along this radial line.

Nevertheless, due to numerical errors, the successive passages are not *exactly* located on such radial line. Therefore it is preferable to consider another dispersion map, that is the one located along the radial line at θ_2 fixed. Since the results are obtained in the sidereal reference frame, it is more appropriate to express the variance matrix in the polar P_2-centered coordinate system. Doing so, the variance along the radial and transverse direction provide much more useful information, that is the error with respect to the nominal conditions in terms of distance from the surface of Mars and error with respect to the backward or the forward shifting of the position and velocity. Hereafter some exemplification of the analysis performed on all the capture set. For each situation, the overall scenario of the perturbed capture set is presented, then the dispersion map at the reference station and the associated statistical parameters are reported and, eventually, a histogram depicting the outcome of the perturbation in terms of successful perturbed captures, crashes and escapes is shown. This procedure will be repeated for some particular case and, after all, the global results will be analyzed and conclusion will be discussed.

3.3.1 Results for a robust capture set

In Figure 3.5 it is represented a *robust* ballistic capture orbit. From the propagation of the perturbed initial conditions, a quite regular profile is obtained. This is clearly visible from the left part of Figure 3.5. On the right part of the same figure, the corridor created by the superposition of the entire set of orbits is reported. For this particular case, such corridor is 13 km wide. Figures from 3.6a to 3.6f represent all the passages at the selected stations. For each one, an error ellipse has been traced and the variance in the local reference frame (described by the blue and the green arrow, which are nothing but eigenvectors of the covariance matrix associated to

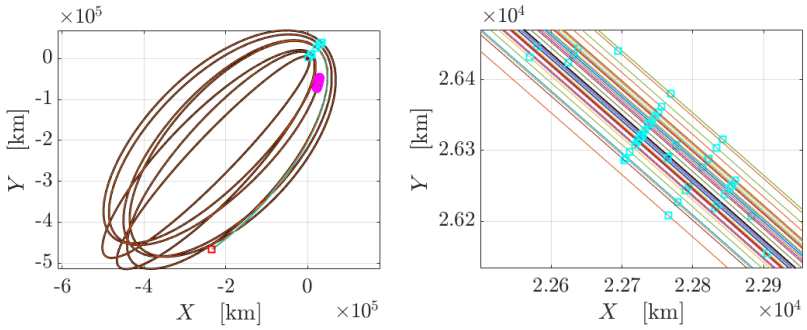

Figura 3.5: Perturbed set of initial conditions from the capure set $\mathcal{C}^6_{-1}(0, 0.90)$ (on the left) and particular of the sixth passage about Mars (on the right). The red square (□) represent the set of initial conditions for this particular perturbed set. The magenta circles (○). Eventually the cyan squares (□) indicate the selected instant in which the spacecraft cross the radial line whose θ_2 corresponds to the first close passage.

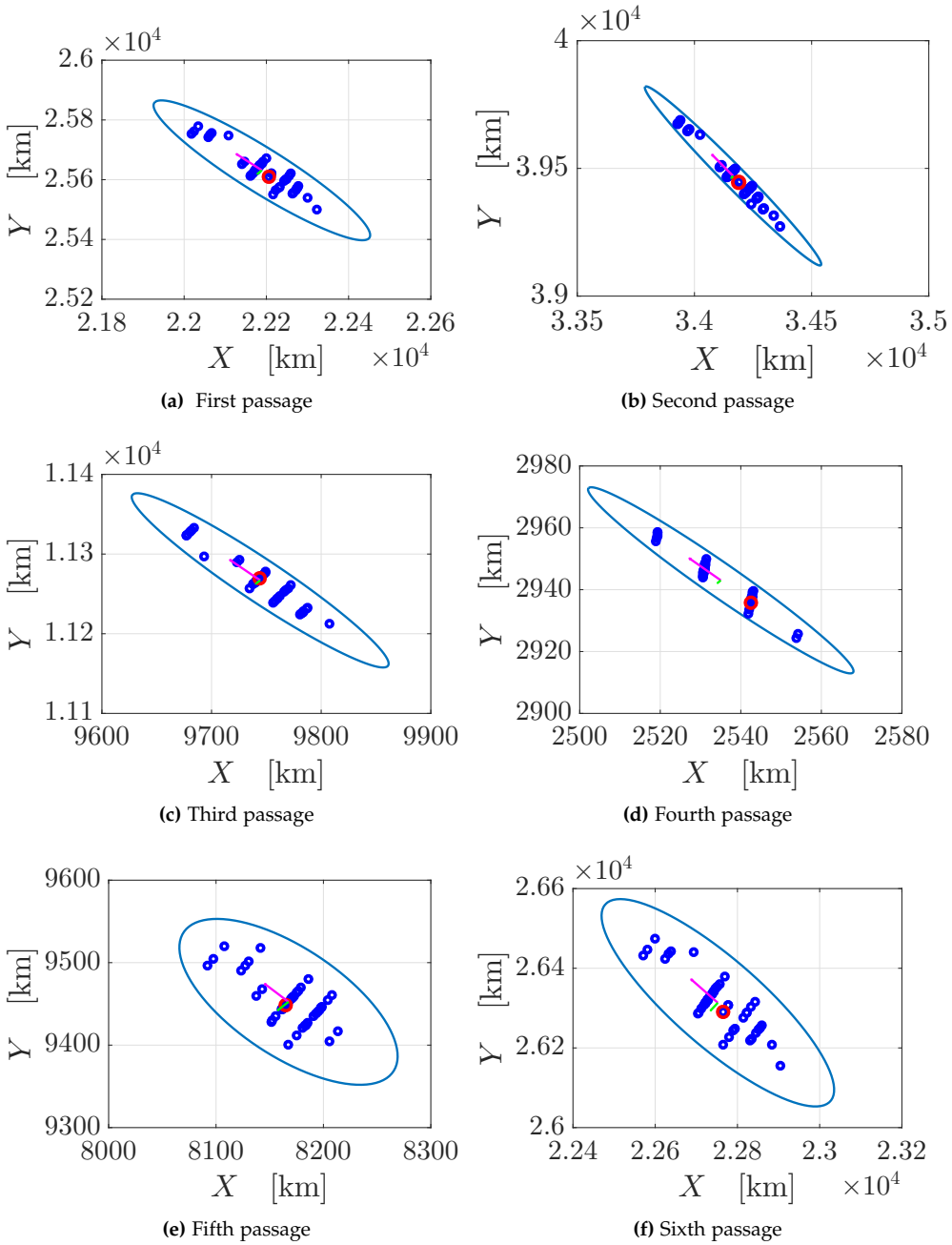

(a) First passage **(b)** Second passage

(c) Third passage **(d)** Fourth passage

(e) Fifth passage **(f)** Sixth passage

Figura 3.6: Dispersion maps of the perturbed capture sets at the reference station

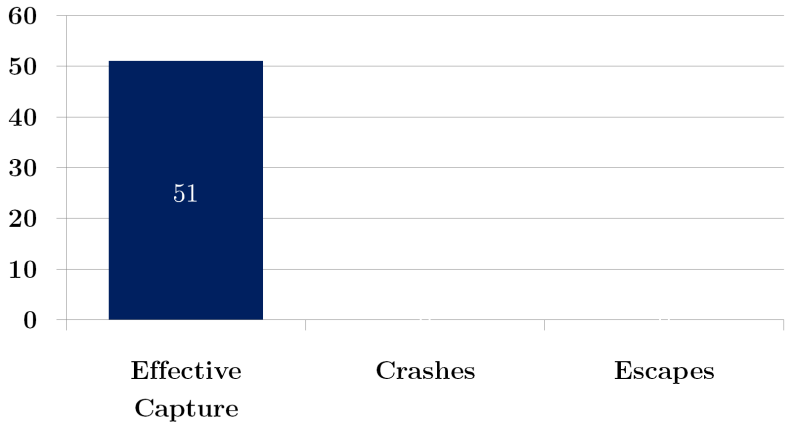

Figura 3.7: Count of orbit typology.

Figura 3.8: Summary plot of the principal evidence for a particular set of perturbed initial conditions inside the set $\mathcal{C}^6_{-1}(0, 0.90)$.

the maximum and the minimum eigenvalue) points out the count of initial conditions which produce a successful ballistic capture, a crash of an escape. According to this situation, nothing but regular behavior occurs. For sake of completeness, the diagonal variance matrices of the error ellipse represented in Figures 3.6a to 3.6f are hereafter reported. They have been obtained by simply rotating by the angle δ (defined in eq. 3.8) the non-diagonal variance matrix obtained from the data set $[X, Y]$ at the various close passages. Therefore, by labeling $\boldsymbol{R}$ the rotation matrix:

$$\boldsymbol{R} = \begin{bmatrix} \cos(\delta) & \sin(\delta) \\ -\sin(\delta) & \cos(\delta) \end{bmatrix} \tag{3.9}$$

The diagonal variance matrix $\hat{\boldsymbol{\sigma}}$ stems from:

$$\hat{\boldsymbol{\sigma}} = \boldsymbol{R}\boldsymbol{\sigma}\boldsymbol{R}^T \tag{3.10}$$

The diagonal matrices for the case under analysis are:

- First passage:
$$\boldsymbol{\sigma}_1 = \begin{bmatrix} 8293.8 & 0 \\ 0.0000 & 308.8 \end{bmatrix}$$
- Second passage:
$$\boldsymbol{\sigma}_2 = \begin{bmatrix} 18176 & 0 \\ 0.0000 & 132 \end{bmatrix}$$
- Third passage:
$$\boldsymbol{\sigma}_2 = \begin{bmatrix} 1740.5 & 0 \\ 0.0000 & 38.8 \end{bmatrix}$$

- Fourth passage:

$$\boldsymbol{\sigma}_2 = \begin{bmatrix} 136.32 & 0 \\ 0.0000 & 1.67 \end{bmatrix}$$

- Fifth passage:

$$\boldsymbol{\sigma}_2 = \begin{bmatrix} 1171.7 & 0 \\ 0.0000 & 243.7 \end{bmatrix}$$

- Sixth passage:

$$\boldsymbol{\sigma}_2 = \begin{bmatrix} 9415.6 & 0 \\ 0.0000 & 818.4 \end{bmatrix}$$

The same procedure can be applied to an acrobatic set in order to show its robustness. Hereafter it is reported, as further example, the results obtained from the perturbation of an initial condition contained in the set $\mathcal{C}^6_{-1}(0.50\pi, 0.99)$.

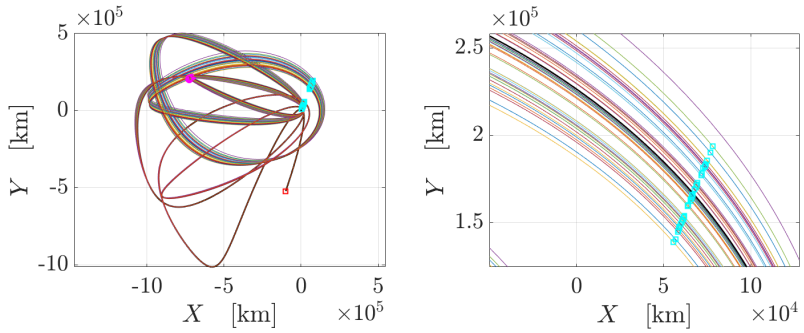

Figura 3.9: Perturbed set of initial conditions from the capure set $\mathcal{C}^6_{-1}(0.50\pi, 0.99)$ (on the left) and particular of the sixth passage about Mars (on the right). The red square (□) represent the set of initial conditions for this particular perturbed set. The magenta circles (○). Eventually the cyan squares (□) indicate the selected instant in which the spacecraft cross the radial line whose θ_2 corresponds to the first close passage.

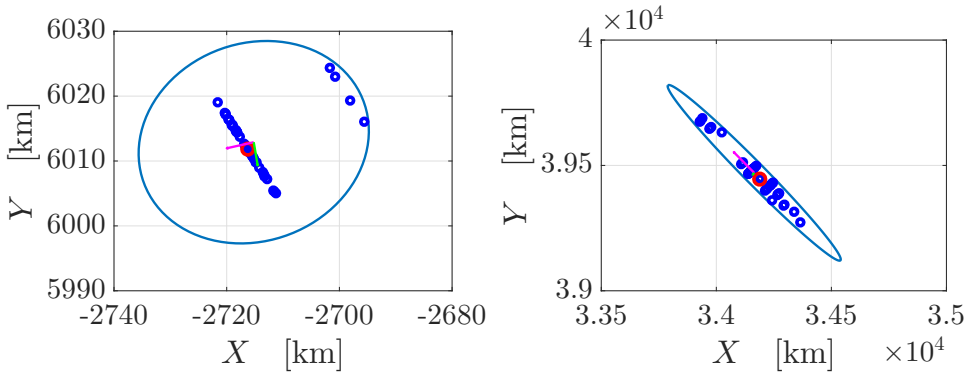

(a) *First passage* **(b)** Second passage

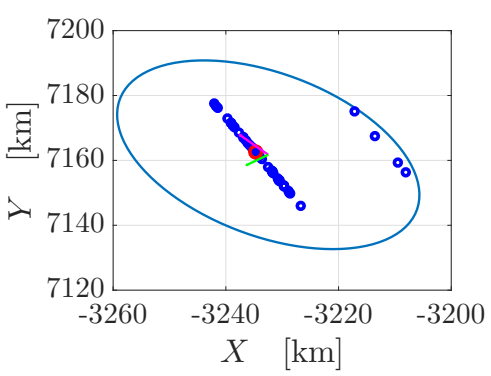

(c) Third passage

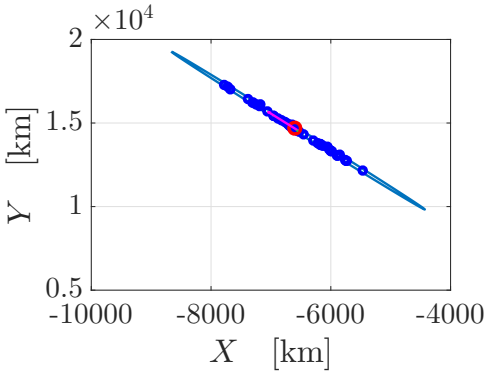

(d) Fourth passage

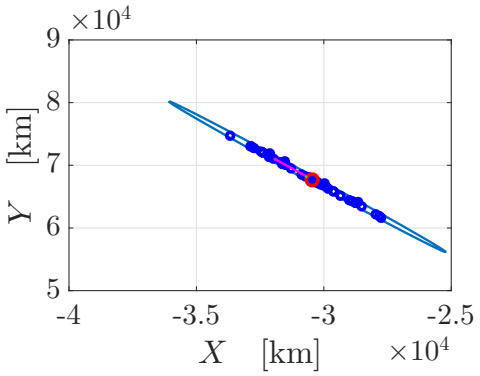

(e) Fifth passage

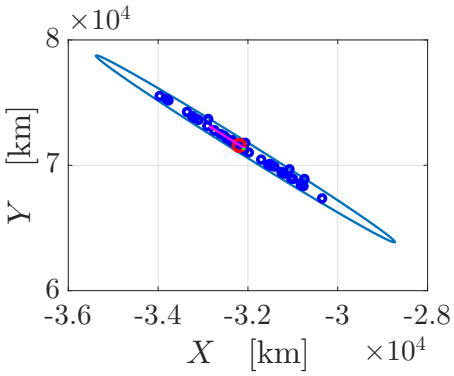

(f) Sixth passage

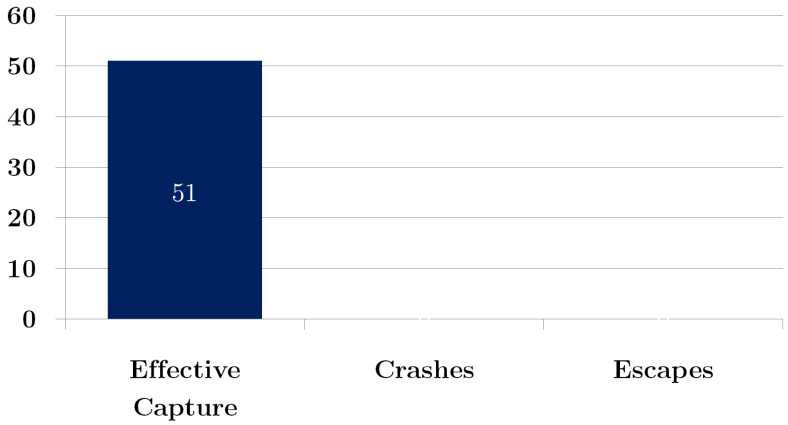

(g) Count of orbit typology.

Hereafter the variance matrices are reported:

- First passage:

$$\boldsymbol{\sigma}_1 = \begin{bmatrix} 29.3875 & 0 \\ 0 & 16.3784 \end{bmatrix}$$

- Second passage:
$$\boldsymbol{\sigma}_2 = \begin{bmatrix} 3055.7 & 0 \\ 0 & 576.8 \end{bmatrix}$$
- Third passage:
$$\boldsymbol{\sigma}_2 = \begin{bmatrix} 77.6478 & 0 \\ 0 & 30.7722 \end{bmatrix}$$
- Fourth passage:
$$\boldsymbol{\sigma}_2 = \begin{bmatrix} 1853400 & \\ & 200 \end{bmatrix}$$
- Fifth passage:
$$\boldsymbol{\sigma}_2 = \begin{bmatrix} 1202500 & 0 \\ 0 & 400 \end{bmatrix}$$
- Sixth passage:
$$\boldsymbol{\sigma}_2 = \begin{bmatrix} 46200000 & 0 \\ 0 & 4400 \end{bmatrix}$$

It is possible to note that the shifting with respect to the nominal condition strongly increases as the integration goes forward. This allows to think that a further propagation of motion beyond the *six-time-stable* limit could produce an escape or a destructive event over the surface of Mars. However, for the true anomaly span considered, even acrobatics orbits can be robust. As done before, the dispersion maps at the passages at the reference stations have been represented and the variance matrices describing the magnitude of the shifting with respect to the nominal conditions have been reported. Being the dispersion maps much wider with respect to the previous case, the values of the variance strongly increase. It must be noted that it has made a comparison between two capture set belonging to the two *end sets* and all the phenomena associated to the increase in the true anomaly and the eccentricity of the osculating orbits have produced.

3.3.2 Results for a non-robust capture set

The analysis performed in the previous section has been applied also to *non-robust* ballistic capture orbits, that is orbits whose perturbed initial conditions produce an escape path or a crash over the surface of Mars. Of course a non-robust orbit cannot be considered a good candidate for a ballistic capture, at least not in the framework of an unperturbed dynamics (both in the sense of environmental perturbation and on board propulsion[4]) where the motion occurs just for purely gravitational interaction between the spacecraft and the primaries. Therefore in this section, some example of initial conditions which *cannot* be used are presented.

Among the non-suitable initial conditions it is possible to distinguish three main groups:

[4] Which corresponds to the possibility to perform OCM.

- Initial condition producing almost the same amount of capture, crashes and escapes;

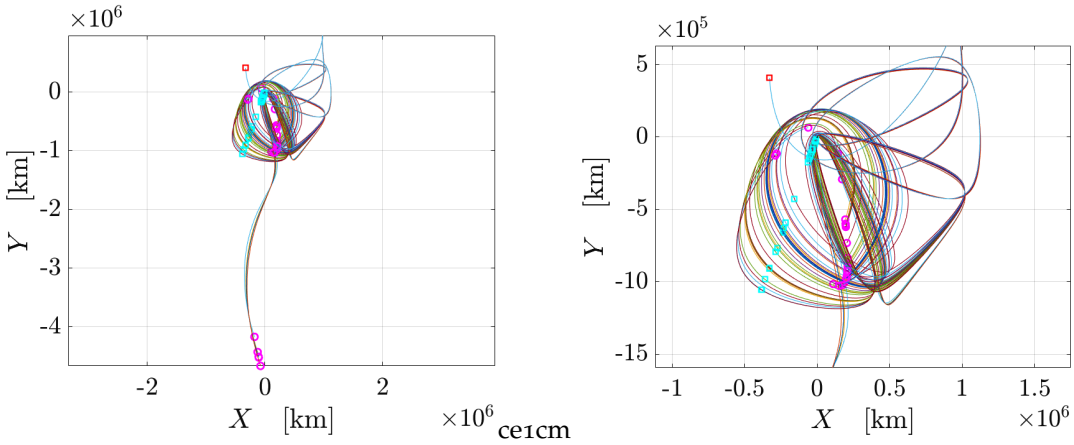

(a) Overview **(b)** Particular

Figura 3.9: Set of initial condition taken from $\mathcal{C}^6_{-1}(0, 0.90)$ producing 22 captures, 16 crashes and 13 escapes.

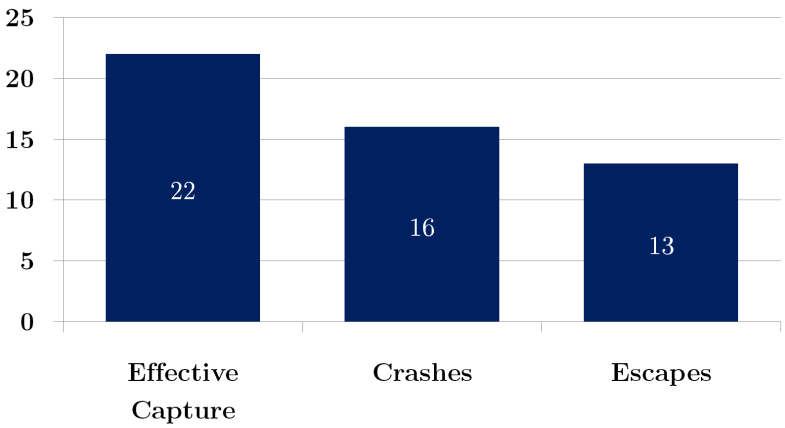

Figura 3.10: Count of orbit typology.

- Initial conditions more prone to produce crashes;

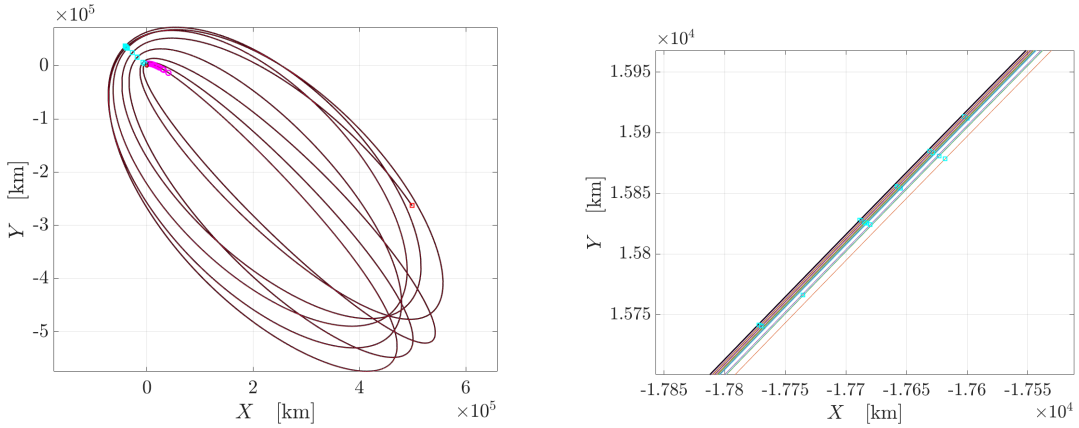

(a) Overview **(b)** Particular

Figura 3.11: Set of initial condition taken from $\mathcal{C}^6_{-1}$ (0.50π,0.90) producing 22 captures, 29 crashes and no escapes. It must be noted that the dispersion map in (3.11b) very little populated. This is due to the fact that orbits leading to crashes have been directly discarded and, consequently, not plotted.

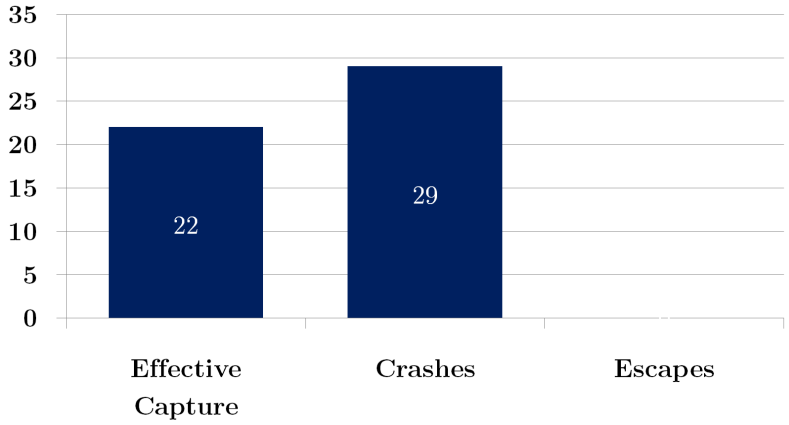

Figura 3.12: Count of orbit typology.

- Initial conditions leading most to an escape.

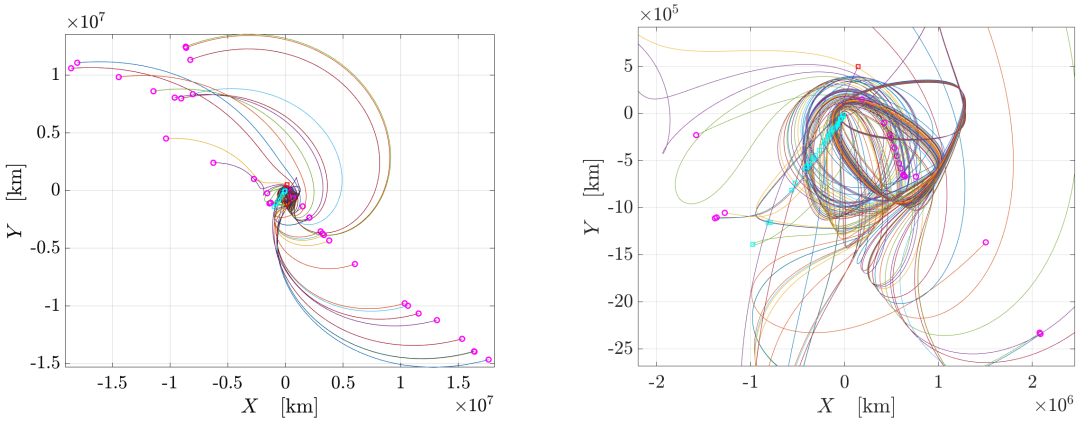

(a) Overview **(b)** Particular

Figura 3.13: Set of initial condition taken from $\mathcal{C}^6_{-1}$ (0,0.99) producing 14 captures, 3 crashes and 34 escapes. It can be noted from (3.13b) that this particular set is an acrobatic one and definitely it is not robust with respect to perturbations of the initial state.

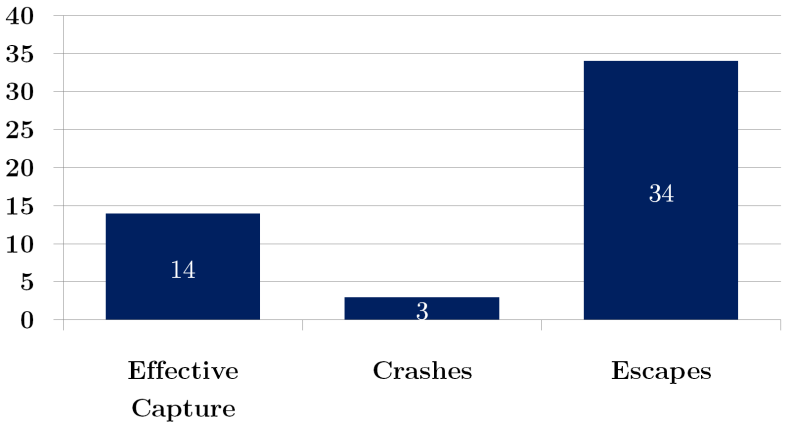

Figura 3.14: Count of orbit typology.

3.4 OVERALL RESULTS AND CONCLUSION

So far, some examples from specific situations have been presented in order to provide a quite detailed overview about the outcomes of the calculation procedure and of the hypotheses that were made. The behavior of the perturbed capture sets, in relation to the current value of initial true anomaly and eccentricity of the osculating orbits, have been analyzed in terms of size and shape of the capture set and of stability[5] of the orbital paths. The statistics used to describe the trend of the perturbed state vector at reference stations has been analyzed as well.

The overall quantitative and qualitative results must be still presented. In this work, 148104 perturbed initial conditions have been generated and each one has been propagated forward and, for each resulting orbit, the robustness have been studied. Table 8 contains the quantitative *summa* of the whole analysis. Numbers presented give an idea about the most robust conditions and to which set they belong.

Tabella 8: Quantitative result of the robustness analys of ballisti capture orbits for the Sun-Earth system in the elliptic restricted three-body problem.

Set ID	Captures	Crashes	Escapes	Total for category
`f000pi_e90`	19003	586	658	20247
`f000pi_e99`	25877	716	1865	28458
`f025pi_e90`	17642	278	287	18207
`f025pi_e99`	27763	614	2070	30447
`f050pi_e90`	12793	561	314	13668
`f050pi_e99`	35492	327	1258	13668
TOTAL	138570	3094	6452	148104

Figure 3.15 and Figure 3.16 provide a graphical representation of the information contained in Table 8.It can be noted immediately that, for each set of perturbed initial conditions, the number of effective ballistic capture is tremendously higher than crashes and escapes. Moreover it can be noted also that a high value of eccentricity not only produces a denser capture set, but makes such set very robust against perturbations.

It must be noted also that the set `f025pi_e90`, despite it is the penultimate in terms of number of initial conditions, it is characterized by the highest percentage of effective captures and the lowest one of escapes. However, in first approximation, the most critical situation is represented by a crash. According to Figure 3.16, the set `f025pi_e90` exhibits the lowest amount of crashes, being also the set with the biggest set of initial conditions. This is a further confirmation of what stated before for the benefits deriving from high value of f and e.

[5] Note that *stability* in this particular case is meant as the shifting with respect to the nominal conditions.

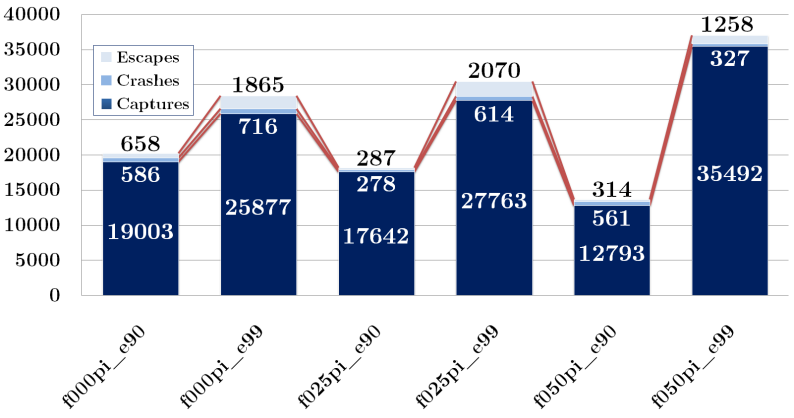

Figura 3.15: Representation of the number of capture/crashes/escapes for each set of perturbed initial conditions.

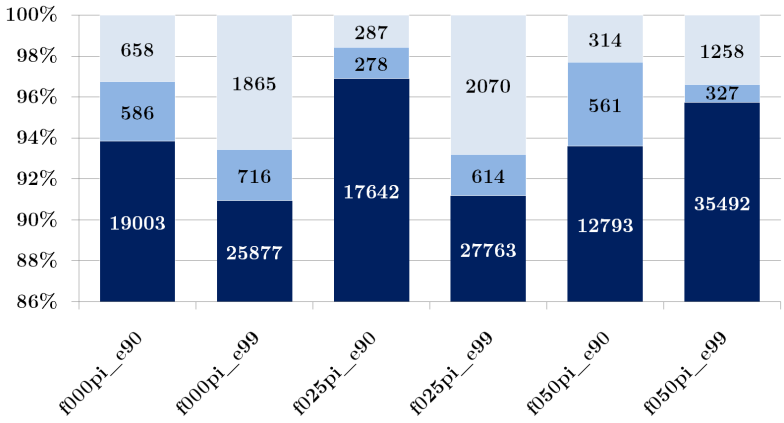

Figura 3.16: Representation of the percentage of capture/crashes/escapes for each set of perturbed initial conditions. The bar coloration criterion is the same as Figure 3.15

As final consideration it can be concluded that the concept of ballistic capture orbits is a very powerful tool for space exploration. With this work it was meant to corroborate the feasibility of a space flight featuring this kind of approach of the target primary. The robustness analysis applied to initial conditions located very far from Mars has shown that, provided that the robust initial condition is matched at the Sphere of Influence, the capture occurs with no need of further corrections in the orbital trajectory.

3.5 FUTURE DEVELOPMENT

This robustness analysis is just a tiny fraction of the huge amount of work that can be developed in the future. The true intention was to set the basis for a methodology to assess the behavior of an enormous collections of initial conditions and to obtain some preliminary results in order to verify the fulfillment of the hypotheses.

The first improvement to this method is the consideration of a *perturbed* environment, both in the deep space phase and nearby the primary. As immediate consequence, a certain amount of OCM might be necessary. However, such maneuvers should be performed *before* meeting the initial conditions at the SOI of Mars, so that no propulsion is necessary during the ballistic capture phase.

The second and most important improvement consist in the exploitation of *differential algebra* to propagate large set of initial conditions, instead of integrating each single state vector. DA is a very powerful tool against the numerous non-linearities which are present in this work. Non linear propagation of uncertainties plays a key role in astrodynamics. Orbit determination is affected by measurement errors; consequently, the knowledge of the state of any spacecraft or celestial body is characterized by an estimable level of uncertainty. Typically these uncertainties need to be propagated forward in time, for example for spacecraft navigation or to estimate the collision risk between artificial satellites or the threat from near Earthobjects. As orbital dynamics is highly nonlinear the size of the uncertainty set tends to quickly increase along the trajectory. Nonl-inearities are not confined to object dynamics: even simple con- versions between different coordinate systems (e.g. the conversion from polar to Cartesian coordinates that forms the foundation for the observation models of many sensors) introduce significant non-linearities and, thus, affect the accuracy of classical uncertainty propagation techniques. An alternative way to map the statistics is based on the approximation of the flow of the dynamics in Taylor series and the use of the resulting polynomials as dynamical substitutes. By using a tool which is based on the *Taylor polynomials expansion*, two great advantage follows: no integration is necessary when the state vector at a certain station is required: the only thing to do is to expand the Taylor series expansion up to the required order at the required location. The higher is the order of the expansion, the more non-linearities are counteracted. Moreover, a lot of computation time is required since, for a purely Matlab environment, a mere integration of the equations of motion is performed. Furthermore, by using this approach, it is no longer necessary to integrate forward the single initial conditions, but it is sufficient to consider an initial box of initial conditions. By considering the Taylor expansion at the required station, it will be produced another box representing the state vector but with a different box shape with respect to the initial configuration due to the fact that a polynomial expansion has been used. This can provide an immediate profile of an outcome which, in Matlab, is obtained only by expensive and time consuming integration. Detailed treatment of this topics which would represent an inestimable improvement to this method are reported in *Wittig* et al. [18] and *Di Lizia*, *Armellin* e *Lavagna* [5].

BIBLIOGRAPHY

[1] Edward Belbruno. *Capture dynamics and chaotic motions in celestial mechanics: With applications to the construction of low energy transfers*. Princeton University Press, 2004.

[2] Edward Belbruno, Marian Gidea e Francesco Topputo. "Weak stability boundary and invariant manifolds". In: *SIAM Journal on Applied Dynamical Systems* 9.3 (2010), pp. 1061–1089.

[3] Edward A Belbruno e James K Miller. "Sun-perturbed Earth-to-Moon transfers with ballistic capture". In: *Journal of Guidance, Control, and Dynamics* 16.4 (1993), pp. 770–775.

[4] Christian Circi e Paolo Teofilatto. "On the dynamics of weak stability boundary lunar transfers". In: *Celestial Mechanics and Dynamical Astronomy* 79.1 (2001), pp. 41–72.

[5] P Di Lizia, R Armellin e M Lavagna. "Application of high order expansions of two-point boundary value problems to astrodynamics". In: *Celestial Mechanics and Dynamical Astronomy* 102.4 (2008), pp. 355–375.

[6] F García e G Gómez. "A note on weak stability boundaries". In: *Celestial Mechanics and Dynamical Astronomy* 97.2 (2007), pp. 87–100.

[7] Nicola Hyeraci e Francesco Topputo. "Method to design ballistic capture in the elliptic restricted three-body problem". In: *Journal of guidance, control, and dynamics* 33.6 (2010), pp. 1814–1823.

[8] Nicola Hyeraci e Francesco Topputo. "The role of true anomaly in ballistic capture". In: *Celestial Mechanics and Dynamical Astronomy* 116.2 (2013), pp. 175–193.

[9] Angel Jorba e Josep Masdemont. "Dynamics in the center manifold of the collinear points of the restricted three body problem". In: *Physica D: Nonlinear Phenomena* 132.1 (1999), pp. 189–213.

[10] Wang Sang Koon et al. "Heteroclinic connections between periodic orbits and resonance transitions in celestial mechanics". In: *Chaos: An Interdisciplinary Journal of Nonlinear Science* 10.2 (2000), pp. 427–469.

[11] Wang Sang Koon et al. "Shoot the moon". In: (2000).

[12] Z-F Luo e F Topputo. "Analysis of ballistic capture in Sun–planet models". In: *Advances in Space Research* 56.6 (2015), pp. 1030–1041.

[13] Z-F Luo et al. "Constructing ballistic capture orbits in the real Solar System model". In: *Celestial Mechanics and Dynamical Astronomy* 120.4 (2014), pp. 433–450.

[14] James K Miller e Edward A Belbruno. "A method for the construction of a lunar transfer trajectory using ballistic capture". In: *Spaceflight mechanics 1991*. Vol. 1. 1991, pp. 97–109.

[15] Victory Szebehely. *Theory of orbit: The restricted problem of three Bodies*. Elsevier, 2012.

[16] Francesco Topputo e Edward Belbruno. "Computation of weak stability boundaries: Sun–Jupiter system". In: *Celestial Mechanics and Dynamical Astronomy* 105.1-3 (2009), pp. 3–17.

[17] V. G. Turyšev. "Basics of Spacecraft Navigation: Principles, methods and observables". In: *Lecture at Jet Propulsion Laboratory, Caltech Institute of Technology* (2011).

[18] Alexander Wittig et al. "Propagation of large uncertainty sets in orbital dynamics by automatic domain splitting". In: *Celestial Mechanics and Dynamical Astronomy* 122.3 (2015), pp. 239–261.